Journal of Chromatography, 648 (1993) 41–69
Elsevier Science Publishers B.V., Amsterdam

CHROMSYMP. 2871

Mechanism of size-exclusion chromatography

I. Role of convection and obstructed diffusion in size-exclusion chromatography

M. Potschka

Porzellangasse 19/2/9, A-1090 Vienna (Austria)

ABSTRACT

Based on experimental evidence, this paper establishes a proper theory of obstructed diffusion which includes the behaviour of polyelectrolytes at low ionic strength and has relevance far beyond chromatography. In addition, it establishes the role of convection in the chromatographic transport process within the porous matrix, which consequently is totally porous and filled with a slowly moving "stagnant" zone. Convection is a crucial factor for the high resolution of modern HPLC columns and size-exclusion chromatographic analysis of ultra-large polymers would be impossible otherwise. Convection processes in the mobile and stagnant zones, of course, are related and a proper description of eddy dispersion thus facilitates understanding of the process within the pores. The processes of dispersion and retention are demonstrated to be governed by different measures of size which delimits the role of transport processes in the mechanism of retention and provides information on the asymmetry of polymer shape by the same experiment. The comprehensive interpretation of chromatographic dispersion facilitates *a priori* modelling of resolution, improves size distribution analysis via straightforward correction of physical dispersion and certainly enriches our physical intuition.

INTRODUCTION

Transport through porous media is of relevance not only to chromatography, but also to heterogeneous catalysis, photographic processes, membrane separations, enhanced oil recovery, organ cultures, cell biophysics and more. Obstructed diffusion has been observed in all instances and has been studied by a variety of methods. Contrary to widespread presumption, however, a proper quantitative theory remains to be identified. Transport may also occur by convection, which is certainly more complex and less well understood, both experimentally and theoretically.

This paper analyses the factors that determine peak width (dispersion) in size-exclusion chromatography (SEC). The simultaneous contribution of a variety of parameters to dispersion can only be disentangled by varying the experimental conditions. Of the many factors, emphasis will be placed on the mass transfer term C (in Van Deemter's terminology), which describes the hydrodynamic process in the so-called stagnant zone within the porous matrix. Traditionally this process is considered to be entirely due to diffusion, in part because it had been assumed that the porous beads contained dead-end pores, a model still found in many textbooks. The parameters that define this obstructed diffusion then can be deduced in order to clarity the theory of diffusion in restricted spaces. Electron microscopy, however, demonstrates that chromatographic media are totally porous (reviewed in ref. 1). The existence of interconnected flow-through capillaries rather than of dead-end pores provides for the possibility that under certain conditions convection augments, or even domi-

0021-9673/93/$06.00

nates, the mass transport. Unrecognized, derived parameters of obstructed diffusion would be in systematic error. Only very limited experimental evidence is available on the latter problem.

The purpose of this study was to illuminate the role of convective mass transfer for standard SEC operation and properly identify it in order to test unambiguously the theory of obstructed diffusion. The present investigation also addresses and revises the mobile zone term A, whose proper functional form and magnitude are crucial for the analysis of convection and diffusion in the stagnant zone, both because the C-term quantitatively depends on proper values for the other factors, and because it conceptually helps to model the equivalent situation of convection in the so-called stagnant zone.

As analysis depends on a proper account of all factors that contribute to peak dispersion and no up-to-date review is available, the subject is introduced in the Theory section. To document the crucial role of convection, its functional terms are facultatively omitted from data analysis. For the sake of clarity and because of uncertainty about their correctness, convective terms are therefore not even included in the Theory section but are introduced in the second part of the Discussion. The Theory section thus provides a refined but still conventional apparatus that the Results section uses for data analysis. The observed inconsistent variability of apparent obstruction is taken as evidence for the occurrence of convection and clearly documents the magnitudes that properly extended theory will have to account for via convection. The first part of the Discussion then compares the experimental results with previously published data on obstructed diffusion and with its relevant theory. Finally, the second part of the discussion explicitly summarizes the emerging understanding of convection in porous matrices.

THEORY

Hydraulic properties of porous networks

Normal chromatography takes place under flow and diffusive and convective properties are closely related to geometric and hydraulic characteristics. One decisive criterion is the regime of flow that one is dealing with: molecular or continuum, laminar, inertial or turbulent. To this end, the ratio of inertial force to viscous force is crucial. This ratio is called the Reynolds number, Re [2], but its numerical significance depends on the geometric topology involved. If we equate the characteristic length with the bead diameter we obtain for the interstitial volume

$$Re = \frac{d\,(\mu\mathrm{m}) \cdot \rho\,(\mathrm{g/ml})}{100 \cdot \eta\,(\mathrm{cP})} \cdot c\,(\mathrm{cm/s})$$

$$= \frac{L\,(\mathrm{cm}) \cdot d\,(\mu\mathrm{m}) \cdot \rho\,(\mathrm{g/ml})}{6000 \cdot V_{\mathrm{void}}\,(\mathrm{ml}) \cdot \eta\,(\mathrm{cP})} \cdot \mathrm{flux}\,(\mathrm{ml/min}) \quad (1)$$

where ρ is the fluid density, η its viscosity and c the actual mean linear fluid velocity in the interstitial space, which should not be confused with the superficial velocity defined for the equivalent empty column. Unfortunately, some workers even interchange the labels for the various possible definitions of velocity (see, e.g., ref. 3). The column parameters are given in Table I.

The use of the total liquid flux in eqn. 1 assumes that flow through the pores contributes a negligible volume. This will be justified below. Under normal operating conditions $Re < 0.01$ and the extremal value that can be reached with say TSK6000PW is $Re = 0.04$. This is well within $Re < 0.1$, which is considered the laminar regime dominated by viscous forces [4]. This is also the region of geometric scaling. Inertial effects are said to become dominant for $Re > 1$ and turbulence starts at *ca.* $10Re$ for packed beds [5] and much later for open-tubular capillaries. The Reynolds number for the pores is always smaller than that of the interstitial volume given above. With liquids one is dealing with the continuum regime, as the mean free path length in liquids is of the order of ångstroms, *i.e.*, much smaller than the dimensions of the pores.

Chromatographic columns contain two sizes of cavities, the interstitial space and the pores proper, in parallel across the same pressure drop. According to the Hagen–Poiseuille equation [6–8], the ratio of the flow-rates is proportional to the square of the ratio of their radii. The radius of the cavity created by spherical

TABLE I

COLUMN PARAMETERS

Property	Symbol and units	TSK6000PW	TSK5000PW	Superose-6	Superose-12
pH stability range	pH	2–12	2–12	1–14	1–14
Maximum back-pressure	Δp_{max} (bar)	5	10	10	20
Shape of beads		Spherical	Spherical	Spherical	Spherical
Bead diameter	d (μm)	25 (±5)[a]	17 (±2)[a]	13 (±2)	10 (±2)
Column length	L (cm)	60	60	30	30
Total column volume	V_{column} (ml)	26.5	26.5	23.6	23.6
Total liquid volume	V_{tot} (ml)	23.0	21.85	21.75	19.5
Interstitial volume	V_{void} (ml)	*ca.* 10[b]	10.2	7.0	7.6
Interstitial porosity	$p_i = \frac{V_{void}}{V_{column}}$	*ca.* 0.38[b]	0.38	0.30	0.32
Bead porosity	$p_b = \frac{V_{tot} - V_{void}}{V_{column} - V_{void}}$	0.87	0.71	0.89	0.74
Tortuosity factor[c]	ξ_1/p_b	1.22	1.71	1.18	1.60
Maximum pore radius[d]	R_{max} (nm)	*ca.* 370	55	27	13
Average pore radius[e]	$R_{1/2}$ (nm)	*ca.* 125	36	25	14
Convective factor	$Cf = \frac{10^6 \cdot [d\,(\mu m)]^2}{9 \cdot [R_{max}\,(nm)]^2}\left(\frac{p_i}{1-p_i}\right)^2$	190	4000	4700	13 000

[a] Note that TSK-PW columns are now sold with modified specifications [145].
[b] Based on similar values for TSK5000PW.
[c] Using eqn. 17 with p_b.
[d] Measured from the minimum size R_{SEC} of solutes that still elute at V_{void} under conditions where interfacial repulsion R_{IF} is a minimum but without correcting for it. The true R_{max} and pore size distribution are therefore larger than suggested by the table.
[e] From ref. 72, with revision.

beads may be approximated from the diameter of the bead as [9,10]

$$r_i = \frac{d}{3} \cdot \frac{p_i}{1-p_i} \quad (2)$$

where p_i is the interstitial porosity and d is the z-average bead diameter. Close random packing is not required. Interstitial porosity is a trivial measure of the quality in packing the column and is independent of bead size. In the literature a value of $p_i = 0.36$ is considered an optimum close random packing of spheres [9,11]. For comparison, hexagonal close packing yields $p_i = 0.26$ [12]. Pore radii are measured chromatographically and typical values are listed in Table I. The ratio of the interstitial flow-rate to the flow-rate inside the pores is thus introduced as the convective factor:

$$Cf = \frac{10^6 \cdot d^2\,(\mu m)}{9 \cdot R_{max}^2\,(nm)}\left(\frac{p_i}{1-p_i}\right)^2 \quad (3)$$

Typical Cf values are listed in Table I. Clearly, most of the liquid flow is due to the interstices between the beads in all instances. This is supported by the observation that the pressure drop Δp is the same for equally sized beads regardless of their pore size [13].

Judged by the Cf values, the liquid of the porous network within the beads is effectively stagnant. This justifies the standard model of SEC in spite of flow-through capillaries, namely a parallel process of flow between the beads and diffusion into a stagnant liquid inside the beads. However, the finite flow that nonetheless is present in the quasi-stagnant zone may augment diffusion via convective transport. The role of convection within the pores is therefore to be judged by comparison with diffusion rates and not with bulk flow. A traditional measure of diffusion rate is the Peclet number, specified below, which assumes a standard three-dimensional random walk. Numerical factors aside,

convection dominates the distribution of solute inside the porous network of the beads whenever the Peclet number *Pe* exceeds the convective factor *Cf*. According to this rationale the dominant mode of solute transport in the so-called stagnant zone is expected to be convection for TSK6000PW but diffusion for Superose-12 (Table I). Fig. 1 illustrates the situation. The onset of convection is most easily recognized by analysing peak dispersion. This analysis, which is presented in the Results section, suggests that convective transport already contributes in the case of Superose-6.

To reduce peak dispersion it is obviously sufficient that the largest pores distribute solute within the bead by convection. The intervening region of smaller pores left by the larger ones forms microbeads with significantly reduced effective bead diameter. It is for this reason that eqn. 3 was based on R_{max} and not on $R_{1/2}$. Recently novel media have been synthesized that contain a mixture of small and ultra-large pores to take advantage of these hydraulic properties. This "perfusion chromatography" [14,15], as it was called, resembles the properties of conventional wide-pore SEC media as discussed above.

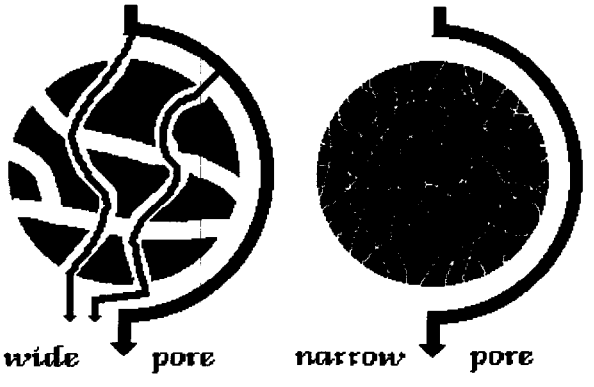

Fig. 1. Schematic diagram of a porous bead as used for packing SEC columns. All types of beads are totally porous and contained well connected flow-through capillaries. In principle there is always some liquid flow through the interior channels of the bead. If these pores are narrow the amount of this flow is insignificant and all of the observed flow of a column passes around the bead. Materials then enter the pores exclusively via diffusion. If the pores are wide some relevant fraction of liquid flow passes through the pores themselves. This provides for convective transport of materials into the beads.

The maximum radius R_{max} of these media (Poros; PerSeptive Biosystems, Cambridge, MA, USA) is only slightly larger than that of TSK6000PW, but $Cf > 40$ for the smallest bead size available.

Van Deemter equation

In the following, extra-column instrumental dispersion will not be dealt with and is assumed to be zero for the experimental data presented. Further, the number of plates is high in all instances. In the limit of geometric scaling, classical dispersion analysis then focuses on the reduced Van Deemter master equation. It has been derived in many different ways both from rate theory and from statistical theory. The reduced plate height h is given as [16]

$$h = \frac{L}{dN} = \frac{10^4}{5.54} \cdot \frac{L\,(\mathrm{cm})}{d\,(\mu\mathrm{m})} \left[\frac{w_h\,(\mathrm{ml})}{V\,(\mathrm{ml})}\right]^2$$

$$= A + \frac{B}{Pe} + CPe + P \qquad (4)$$

where L is the column length, d the diameter of the packing beads, N the number of plates in the column, V the retention volume, w_h the peak width at half-height and Pe a reduced velocity called the Peclet number, which is a measure of the ratio of diffusion time per bead to the flow time across the same distance times a numerical factor [2]. Like the diffusion coefficient, it depends on fluid viscosity and temperature. For water at room temperature (20°C), one obtains

$$Pe = \frac{dc}{D} = 0.777 \cdot \frac{L\,(\mathrm{cm}) \cdot d\,(\mu\mathrm{m})}{V_{void}\,(\mathrm{ml})}$$

$$\cdot \mathrm{flux}\,(\mathrm{ml/min}) \cdot R_s\,(\mathrm{nm}) \qquad (5)$$

where R_s is the diffusional Stokes radius and the other variables are column parameters defined in Table I together with representative numerical examples. A, B, C and P are functions that will be discussed below. If the baseline peak width w, defined at the 4σ level, is used a different numerical factor applies [17]. In the Van Deemter equation, the use of the Peclet number allows data obtained with different-sized solutes, different flow-rates and different columns to be combined into a single master curve. Similarly, the

reduced plate height eliminates trivial column variabilities. Representative experimental Van Deemter plots are presented in the Results section. In the following the functional form of the Van Deemter terms is summarized with due account of diverging views.

P-term

P is a measure of sample polydispersity and depends on the selectivity, *i.e.*, the slope of the calibration graph for retention [18–20]:

$$P = \frac{L}{d} \cdot \frac{\ln\left(\frac{M_w}{M_n}\right)}{V^2} \left(\frac{\partial V}{\partial \ln M}\right)^2$$

$$= 10^4 \left(\frac{1+a}{3}\right)^2 \frac{L\,(\mathrm{cm})}{d\,(\mu\mathrm{m})} \cdot \frac{\frac{M_w}{M_n} - 1}{[V\,(\mathrm{ml})]^2} \left[\frac{\partial V\,(\mathrm{ml})}{\partial \ln R_\eta}\right]^2 \quad (6)$$

where a is the Mark–Houwink exponent. P dominates in eqn. 4 whenever $M_w/M_n > 1.01$ and then obscures the other parameters. Hence essentially monodisperse samples are required for a meaningful analysis of dispersion.

A-term convection

Giddings [21] lists at least four additive factors for eddy dispersion (convective mixing) in the mobile zone, namely, velocity differences at different radial positions within a capillary, velocity differences amongst different nearby channels due to geometric factors, velocity differences in different regions due to variable packing quality and velocity differences at different radial positions of the packed bed column due to flow distortions near the column wall. Originally Van Deemter assumed that the sum of these, called the A_e-term, is a constant whose value depends on the quality of the packing. Huber, Horváth and Giddings then independently established that each convective subprocess is counteracted by diffusion. Giddings famous coupling equation reads [21]

$$A = \sum_i \left(A_i^{-1} + \frac{\omega_i}{Pe}\right)^{-1} \quad (7)$$

where A_i remains a constant characteristic for each subprocess and ω_i is a proportionality constant. The coupling constant for intra-capillary effects is large of the order of $\omega_1 \approx 100$ and causes an extended Pe dependence, whereas all other coupling constants are small and the Pe variation is significant only below $10Pe$. A different form for A was derived by Huber [22]:

$$A = (A_e^{-1} + \omega' Pe^{-k})^{-1} \quad (8)$$

where $k = 0.5$ and A_e was also considered to be a constant. Horváth and Lin [23] derived the same with $k = 0.33$. Knox and co-workers used an empirically determined k ranging from 0.2 to 0.5 [24] or alternatively an unlimitedly growing function [25,26]:

$$A = A_e = A'' Pe^{0.33} \quad (9)$$

with A'' depending on the quality of the column packing. Ideally its value was 0.5–1 but could possibly reach 5 or greater. By just varying the flow-rate at constant solute size, others sometimes found larger exponents [27], as would be expected in certain instances from eqn. 14 discussed below. For infinite diameter columns exponents as low as 0.2 were found [28,29]. Koch and Brady [16,30] presented a theoretical computation, which scales with p_i but whose simplifications are strictly valid only in the limit $p_i \rightarrow 1$. They demonstrated that eddy dispersion will increase unlimitedly with Pe under the assumption of a viscous regime owing to the formation of boundary layers that are inaccessible to convection [16,30]:

$$A_e = 1.5\left(1 + \varepsilon \cdot \frac{V_{\mathrm{column}} - V_{\mathrm{void}}}{V_{\mathrm{column}}} \cdot \ln Pe\right) \quad (10)$$

with the computed value $\varepsilon = 2.2$ for ideally smooth spheres. A rougher surface should have a smaller ε. The factor 1.5 represents the computational situation; in practice, A_e seems to depend on the quality of packing and the complex functional origins of the prefactor are poorly understood. The constant term is equivalent to the sum of the low-coupled convective contributions. A_e also depends on column diameter if the ratio of column diameter to bead diameter is less than 100 [31–33]. More importantly, A_e is a sensitive function of the bead size distribution

and dramatically increases with modestly increasing size heterogeneity [20,34]. Note that the natural logarithm, the cube root and the coupling equation with suitable constants produce similar trends. The logarithmic dependence originates from the boundary conditions and is related to the thickness Δr of the boundary layers formed (eqn. 14). Reanalysis of dispersion data published by Basedow *et al.*[35] for non-porous pieces of broken glass ($p_i = 0.48$) yields $\varepsilon \approx 0.5$ for different-sized solutes at normal flow-rates, albeit the tortuosity was $\xi_i = 2.0$. This margin increases to $\varepsilon \approx 1.0$ if small solutes at varying flow-rates are used instead and demonstrates that the conditions of flow in packed beds are not laminar, *i.e.*, the ln *Pe* dependence in eqn. 10 is an oversimplification. This important result demarcates and identifies the failure of geometric scaling in liquid chromatography. In fact, ε in eqn. 10 becomes a function of flow-rate, namely

$$\varepsilon \propto c^{m-0.33} \approx c^{0.2} \tag{11}$$

according to the data of Basedow *et al.* [35]. In the inertial regime A_e goes through a maximum, which is well explained by the Taylor–Aries theory and was observed experimentally in one case around 30 000 *Pe*, albeit the true determinant is the Reynolds number. At Reynolds numbers $Re > 10$ the A_e-term eventually becomes constant [36].

A-term film transfer

Mass transfer of solute into accessible pores is associated with extra diffusive resistance across a boundary layer at the interphase between the mobile and stagnant zones just as in any membrane diffusion experiment. The added diffusive contribution to the mobile zone mass transfer was estimated by Wakao and Funazkri, who correlated empirical data, as follows (reviewed in ref. 16):

$$A_p = 1.5\left(\frac{V - V_{void}}{V}\right)^2 \frac{V_{void}}{V_{column} - V_{void}} \cdot \frac{Pe^{0.4}}{1 + 9Pe^{-0.6}} \tag{12}$$

Over the range of typical experimental values, the last term roughly corresponds to $Pe^{0.6}$. Typically, a small totally included molecule ($V = V_{tot}$) has $Pe \approx 10$ and $A_p \approx 0.2$. A_p may increase to about 1 in the middle of the separation range and then decreases back to about 0.3 for the largest molecules. It vanishes at the void. Huber [22] reported a similar term but with $A_p \propto Pe^{0.5}$. According to film theory [16,37],

$$A_p = 13 \cdot \frac{V_{tot} - V_{void}}{V_{void}} \cdot \frac{\Delta r}{d} \cdot CPe \tag{13}$$

where Δr is the thickness of the boundary layer, which depends on the effectiveness of convective mixing and decreases with increasing solute size as [38–43]

$$\Delta r \propto \frac{D_{bulk}^{0.33}}{[c(\mathrm{cm/s})]^m} \tag{14}$$

where c is the stirring speed and $m = 0.33$ for laminar flow, $m = 0.50$ for convective conditions and $m = 0.75$ for turbulent flow. Eqn. 14 is related to the Nusselt number. For $m \approx 0.4$, one effectively obtains $A_p \propto Pe^{0.6}$, in agreement with typical experimental values and with eqn. 12. In eqn. 13, C is the Van Deemter coefficient (see, *e.g.*, eqn. 21) and explicitly includes obstructed diffusion which is hidden in the empirical correlation of eqn. 12. As film theory does not quantitatively predict the magnitude of Δr, eqn. 12 was used in subsequent analysis. A_p should be serially added to the other dispersion terms. Note that according to eqn. 14 either ε in eqn. 10 will become a function of flow rate or *Pe* becomes multiplied by a novel term except for laminar conditions. The same holds for A_p in eqn. 12 or 13.

A-term final equation

Most frequently a single coupling term of the sums of various convective and diffusive contributions is used empirically to which the boundary layer resistance is added serially [16,44]:

$$A = \left(A_e^{-1} + \omega \cdot \frac{B}{Pe}\right)^{-1} + A_p \tag{15}$$

where B is the Van Deemter B-term and ω is a proportionality constant that depends on the column diameter. For column diameters in excess of 100 bead diameters, one theory gives a constant $\omega = 0.55$ due to dominant radial diffu-

sion [33]. Judged by experimental data [45], $\omega B \approx 0.5$ and the coupling is only significant for poorly packed columns at low *Pe*. Others claimed a higher experiment derived limiting value of $\omega = 1.2$ [31]. Clearly, the experimental patterns are dominated by the low-coupling events. This is no problem for the present data analysis, which explicitly includes the second coupling region in the form of a *Pe*-dependent A_e (eqn. 10). A_p is taken from eqn. 12 and $\omega B = 0.5$. The appropriateness of eqn. 15 with a single coupling term in the form chosen could not be validated with the available data at $Pe > 10$.

B-term

Excluding adsorption effects, the Van Deemter coefficient for axial diffusion in SEC may be explicitly written as [16]

$$B = 2\left(\xi_i^{-1} + \xi_p^{-1} \cdot \frac{V - V_{void}}{V_{void}} \cdot \frac{D_{pore}}{D_{bulk}}\right) \quad (16)$$

where D_{pore}/D_{bulk} measures the increased friction in confined spaces. The same term appears in the *C*-coefficient and will be discussed below. Earlier treatments ignored the second term in *B*, which is due to diffusional spreading inside the pores (see, *e.g.*, ref. 22). The factor 2 comes from the proportionality between the diffusion coefficient and the mean distance travelled by a random walk. Considering realistic values for the tortuosity ξ (see below), *B* typically equals 2 and is certainly less than 4 for all practical circumstances. Hence the term may be ignored for $Pe > 10$.

Tortuosity

The ratio by which the curved path a particle has to take through a porous network is longer than the linear end-to-end distance is called tortuosity. In the absence of actual measurements one may assume $\xi = 1.5$ and *i* and *p* refer to the interstitial and pore space, respectively. This coincides with the value for minimal surfaces of cubic symmetry [46]. For an unbounded solution, $\xi = 1$ by definition. Theoretically, the tortuosity in a network of cylindrical pores is [47]

$$\xi_1^{-1} = 1 - \frac{2}{3}(1+p)(1-p)^{3/2} \quad (17)$$

where *p* is the porosity. The limiting value for a cylinder with negligible diameter is $\xi = 3.0$ [46]. In addition to an increased path length, the cross-section of real pores is not constant. Its variation leads to constrictions of the flow path and yields an additional geometric factor [21,48]:

$$\xi_2 = \langle A \rangle \left\langle \frac{1}{A} \right\rangle \quad (18)$$

where $\langle A \rangle$ is the average over the local pore cross-section. ξ_2 increases as the ratio of maximum to minimum cross-section increases [49]:

$$\frac{A_{max}}{A_{min}} = \left(\frac{R_{max}}{R_{min}}\right)^2 \approx 1.6(\xi_2)^3 \quad (19)$$

For closely packed beds of spheres one typically finds $\xi_2 \approx 1.3$, which corresponds to almost a fourfold difference between maximum and minimum cross-sections [49]. The interstitial tortuosity is then simply the product $\xi_i = \xi_1 \xi_2$, but the particular values of $\xi_i = 2.4$–2.6 calculated for the columns in Table I are surprisingly high.

In those instances where the pore volume fraction enters the measurement, such as for the stagnant zone mass transfer, the excluded volume term is added to the obstruction factor whilst nominal porosity is added to tortuosity [50]. The empirical tortuosity coefficient should then be considered to be the product of tortuosity in its primary meaning of constriction and of porosity, *i.e.*,

$$\xi_p = \frac{\xi_1 \xi_2}{p_b} \quad (20)$$

Theoretical values of ξ_1/p_b are listed in Table I. In practice, ξ_p is often derived from the intercept of semi-logarithmic obstructed diffusion relationships, which is sensitive to systematic errors. ξ^{-1} is called the intrinsic conductivity but some workers have labelled it tortuosity instead. Tortuosity is a constant for a given porous structure.

C-term

Finally, for a rate-limiting diffusion within the pores, $C = C_d$ and one may write for the mass transfer term between mobile and stagnant zone

[16]

$$C_d = \xi_p \cdot \frac{V - V_{void}}{V^2} \cdot \frac{V_{void}}{30} \cdot \frac{D_{bulk}}{D_{pore}} \quad (21)$$

where the factor 30 assumes conditions close to equilibrium [51]. Far from equilibrium (large C-term), eqn. 21 will underestimate D_{bulk}/D_{pore} [52]. Here $V - V_{void}$ may but need not be equal to the real geometric volume that is sterically accessible to the solute, since energetic differences may exist between the mobile and stationary zones. Adsorption, however, is assumed to be absent. The presence of a stationary zone requires a modified form of eqn. 21. Up to this point no real assumption about the mechanism of transport has been made and the apparent diffusion coefficient in the pores may also include factors of convection. It is only a formal choice to express C in terms of two functions instead of expressing D_{pore} in terms of two functions. Facultative omission of convective terms therefore exclusively modifies parameters of obstructed diffusion in whatever term is used (*e.g.*, eqn. 22) and is uncoupled from the remainder of dispersion analysis.

Obstructed diffusion

Occasionally a simple exponential function was advocated for obstructed diffusion [16,53]:

$$D_{pore} = D_{bulk} \exp\left(-\alpha \cdot \frac{R_s}{R_{1/2}}\right) \quad (22)$$

and the wide variation of empirical data (see Discussion) hardly justifies more than a single adjustable parameter. Further, the present results are well represented in this form. It is inherent in the derivation that the radius of the solute should equal the diffusional Stokes radius R_s. We shall investigate below whether this holds experimentally and will actually modify eqn. 22. The disadvantage of this semi-logarithmic approach is that, according to theory, slopes taken below $R/R_{1/2} < 0.1$ and above $R/R_{1/2} > 0.05$ need to be distinguished.

Theory of obstructed diffusion

Initially many chromatographers considered the ratio $\xi D_{bulk}/D_{pore}$ to be merely a constant independent of solute size (see Discussion) [44], even though related fields dealt with size-dependent functions. Two factors play a role, frictional drag (according to Faxen [54]) and steric hindrance (according to Ferry [55,56]). The observed increase in friction is truly a problem of flow line perturbation in the proximity of obstacles, *i.e.*, a hydrodynamic interaction between object and obstacle which increases drag. It should not be viewed as if objects were enlarged in size as this exceeded the pore size in which they are contained by orders of magnitude. Steric hindrance is related to the partition coefficient of SEC but it is usually assumed to be the sterically excluded volume of cylindrical capillaries $(1 - R/R_{1/2})$ [2] according to the geometric model employed in theory.

Renkin [57] was first to combine both terms. All theories so far have assumed ideal cylindrical geometry of pore radius $R_{1/2}$ or parallel plates, where $R_{1/2}$ is replaced by half the distance between the plates, $z/2$. Rectangular geometry yields different functions [58,59] and will not be considered further here. The simplest approach, further, is limited to calculation of the force exerted on spherical objects in axial-symmetric flow. Following Faxen and Renkin, various improvements in calculating this centreline approximation were made [50,57,60–63]. For aspect ratios $R/R_{1/2} < 0.5$, there is general consensus (see Fig. 2a). The initial semi-logarithmic slope is $\alpha = 4.6$ [64]. The centreline approximation is the most widely used formula in the field. An extended solution, that includes integration over all eccentric positions, but still with simplifying assumptions, has been presented by Famularo in ref. 63. It seems to be largely unknown in the field. It has an initial slope of $\alpha = 5.5$ that bends to $\alpha = 7.4$ for $R/R_{1/2} > 0.05$ (see Fig. 2c). Consequently, the neglect of non-symmetrical terms amounts to an unacceptable error. The gradual transitions towards solution (a) is expected since centreline terms become more dominant as the aspect ratio increases. Brenner and co-workers [65–67] confirmed the initial semi-logarithmic slope of $\alpha = 5.5$. Their computation claims validity for $R/R_{1/2} < 0.1$ but starts to deviate from Famularo above $R/R_{1/2} > 0.05$ in an oscillatory manner (see Fig. 2b). This discrepancy remains to be understood on a computational level be-

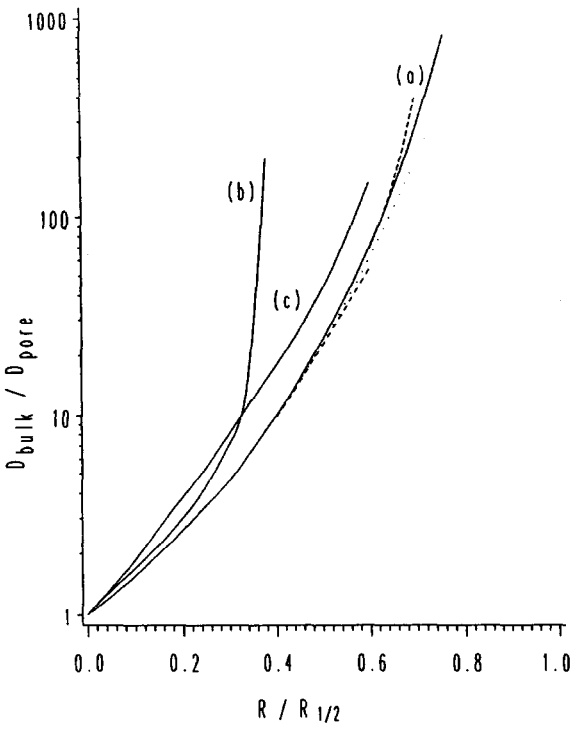

Fig. 2. Theoretical functions for obstructed diffusion in cylindrical tubes with both a drag term and an excluded volume term. (a) Centreline approximations: Faxen and Renkin [57] (lower dashed line), Haberman and Sayre (quoted in ref. 62) (dotted line), Bishop *et al.*, eqn. 12 in ref. 84 (upper dashed line), Paine and Scherr [61] (solid line), all with identical initial slope of $\alpha = 4.6$. (b) Extended solution: Brenner and Gaydos [65], with initial slope of $\alpha = 5.5$. (c) Best solution: Famularo in ref. 63, with initial slope of $\alpha = 5.5$ below $R/R_{1/2} = 0.05$ and with slope of $\alpha = 7.4$ above $R/R_{1/2} = 0.05$.

fore one can be confident that the values of Famularo are correct in all details. There is, however, little reason to doubt the calculation of the initial slope, which thus definitely supersedes the earlier centreline approximation. This is particularly noteworthy, as the initial slope $\alpha =$ 4.6 of the pure centreline approximation has already been claimed to be experimentally verified (see Table IV and its discussion). The rapid rise of Brenner and co-workers' slope (Fig. 2b) above $R/R_{1/2} > 0.3$ is a computational artifact [60] and may have misled the formulation of theory for hydrodynamic chromatography (HDC), where friction bends the calibration graphs backwards for large solutes [68]. Experimental HDC data of this kind are better explained in terms of shear deformation [8]. Mavrovouniotis and Brenner have calculated the limiting case of $R/R_{1/2} > 0.9$, which asymptotically approaches infinity [69]. Scaling theory has been applied to the problem of obstructed diffusion of flexible polymers [70] and tests of its applicability have attracted some interest, but the issue is not decided. Some arguments will be raised in the Discussion section. Note that convective obstruction is much less than diffusional obstruction, especially above $R_s/R_{1/2} > 0.5$ [60].

In comparing data on obstructed diffusion, one must keep in mind that some types of measurement besides SEC are independent of the excluded volume term. For them the pure drag term becomes $\alpha = 3.5$ instead of 5.5 for low aspect ratios. The middle range then should more be of the order of $\alpha = 4.5$ and continues to increase instead of remaining a constant $\alpha = 7.4$ over the entire region. Eqn. 22 is therefore a poor representation of frictional drag variation alone.

Summary

With few exceptions, the *C*-term of the Van Deemter equation for SEC has been exclusively analysed as a diffusion problem. All data on obstructed diffusion obtained from SEC thus lack consideration of convective mass transport, and most were superficial in their treatment of mobile zone factors. To document the role of convection in a model-independent manner, experimental dispersion data are initially analysed with a combination of eqns. 4, 5, 10, 12, 15, 16, 21 and 22. Eqn. 22 eventually will be replaced by eqn. 29 in the Results section. Convective transport modifies D_{pore} and application of eqn. 22 or 29 alone consequently leads to superficially low apparent α values. In this manner the occurrence of convection is easily recognized. Subsequent complete analysis (which is deferred to the second part of the Discussion) then will add eqn. 31 to the above list and test the validity of various proposed theories for C_c (eqns. 30, 33, 36 and 37) with the constraint that the α value should become universal.

EXPERIMENTAL

The instrument, materials and procedures were the same as reported previously [1,71,72]. Peak widths were measured manually off the charts. All reported measurements and theory pertain to the regime of infinite dilution with samples eluting independent of the presence of other components in the case of mixtures. Experience shows that injection volumes should be small and samples to be injected in SEC should not exceed

$$c_{inj} < 0.1[\eta]^{-1} \quad (23)$$

where according to Simha

$$c^* \approx [\eta]^{-1} \quad (24)$$

is called the overlap concentration [70]. For rigid spheres, such as globular proteins, this limit concentration of the dilute solution regime c^* roughly corresponds to the solubility limit. Further, $I \geq 0.002$ M is a lower useful limit for SEC studies since, for the requirement of infinite dilution, the polymer should not contribute significantly to the ionic strength of the eluent:

$$I_{polymer} \approx \frac{n(n+1)}{2} \cdot \frac{c_{inj}\ (mg/ml)}{M} << I \quad (25)$$

where n is the net charge of the polymer. Solute concentrations in excess of eqn. 25 induce concentration gradients of the support electrolyte that increasingly distort the elution profiles. For measurement of peak dispersion it is particularly important that the solvent of the sample and the eluent are identical.

It has been verified that none of the samples studied here changes its structure over the range of solvent conditions employed. Hence no aggregation, dissociation or denaturation takes place and consequently R_s and R_η, each corresponding to conditions of infinite dilution, remain the same. For coiled polyelectrolytes whose intramolecular forces induced continuous structure changes at varying ionic strength, the hydrodynamic constants appropriate for the particular single condition that was studied in their case were used.

Column parameters are given in Table I. Based on these data and the Hagen–Poiseuille equation, the manufacturer of TSK-PW (Toso-Haas, Tonda, Japan) recommends not to exceed 1.2 ml/min and that of Superose (Pharmacia–LKB, Uppsala, Sweden) specifies 1.5 ml/min. Experiments were performed at different flow-rates, not exceeding 0.5 ml/min, at room temperature. Table II shows typical calibration data that relate molecular size to retention volumes. Typically retention volumes and solute sizes are correlated in a semi-logarithmic fashion without recurrence to any particular model of pore geometry. This makes the analysis independent of V_{tot}, whose proper assessment is disputable. In fact, none of the dispersion analysis depends on V_{tot} either.

TABLE II

REFERENCE DATA AND ELUTION VOLUMES ON SUPEROSE-12

Sample[e]	R_s (nm)	R_{SEC}[a] (nm)	Superose-12 V (ml)[b]
TMV	49	62	7.60 (void)
TBSV	17.2		7.80
Phage MS2	13.9		7.80
DNA (195 bp)	9.3	12.6	8.22
NF200TP+[c]	8.9	11.7	8.50
Thyroglobulin	8.6		9.08
β-Galactosidase	6.86		10.48
Apoferritin	6.06		10.72
Immunoglobulin G	5.23		11.77
Alcohol dehydrogenase	4.55		12.30
Alkaline phosphatase	3.30		13.18
Ovalbumin	2.83		13.65
Calmodulin	2.10		14.10
Myoglobin (horse)	1.91		15.28
Vitamin B_{12}[d]	0.75		19.50

[a] Missing values are for spherical particles where $R_{SEC} = R_s$.
[b] I = 200 mM; pH = 8.0; 10 mM Tris–HCl–194 mM NaCl.
[c] Proteolytic fragment of neurofilament NF200, phosphorylated form.
[d] Used to estimate V_{tot}; however, ^2H_2O elutes about 1 ml later.
[e] TMV = tobacco mosaic virus; TBSV = tomato bushy stunt virus.

RESULTS

Operational parameters

All of the data were obtained with essentially Gaussian peaks. The asymmetry was actually

1.1–1.2 for all Peclet numbers and substances. Fig. 3 demonstrates that the peak width w_h and the reduced plate heights depend on the loading concentration and also vary with the age and status of a column. It is therefore crucial that the stability of performance be checked during a series of axial dispersion measurements. High values of h, observed after cleaning the column, may gradually return to normal lower values. Disturbance of the gel bed on changing the entrance frits (a standard operational option for Superose columns), however, may lead to permanent loss of performance. The latter is easily checked in glass columns with coloured substances. Back-flushing usually leads to a recoverable loss of performance. Fig. 3 also shows that plate heights depend on loading concentration. To guarantee comparable experimental conditions, all subsequent data were taken at loads between 1 and 100 μg, where concentration has no influence and the signal-to-noise ratio is still acceptable. Injection volumes were 10–100 μl.

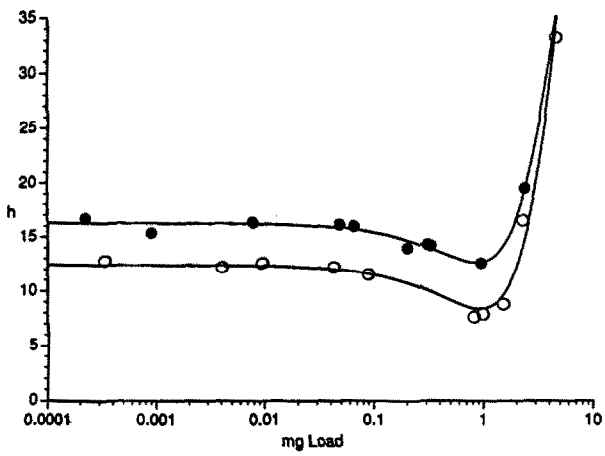

Fig. 3. Dependence of the reduced plate height h on sample load. Here sample load is defined as injection concentration times injection volume. Superose-12 in 10 mM Tris–HCl–94 mM NaCl (pH 8.0, I = 100 mM); flow-rate, 0.4 ml/min; room temperature. Sample, ovalbumin. Two series of measurements at different times but with the same column and conditions resulted in different magnitudes of axial dispersion. ● = Earlier series of measurements; ○ = later series of measurements. Both series employed an injection volume of 100 μl. The loading capacity is *ca.* 2 mg. Viscous fingering was clearly discernible above 10 mg (corresponding to an injection concentration of $c^*/3$).

Proteins are normally monodisperse and thus ideally suited for the analysis of dispersion. Among the exceptions is immunoglobulin, which is polyclonal and is known to contain a mixture of similar sizes of different molecules of variable isoelectric points. Fig. 4 shows that the peak width of immunoglobulin is higher than those of other similar-sized proteins. This is in agreement with the previous statement that even minor

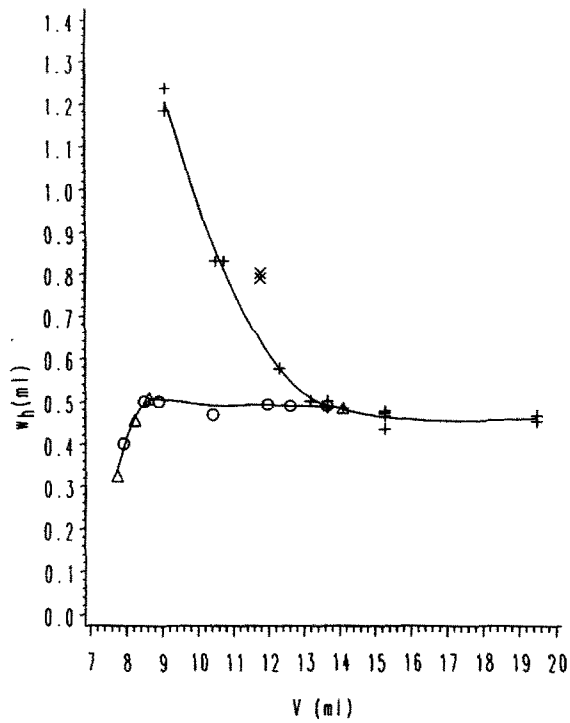

Fig. 4. Axial dispersion for different solutes and conditions on Superose-12 at a flow-rate of 0.5 ml/min, room temperature, buffered aqueous solutions with supporting electrolyte. Shown is the peak width as a function of elution volume. Upper curve: different proteins at I = 200 mM, pH 8.0. From left to right: thyroglobulin, β-galactosidase, apoferritin, alcohol dehydrogenase, alkaline phosphatase, ovalbumin, calmodulin, myoglobin, vitamin B_{12} (+), immunoglobulin G (×). Vertically corresponding marks are repetitive measurements on the same protein. Note that immunoglobulin G, measured under identical conditions, is off the graph because it is heterogeneous. Lower curve: eluents of different ionic strength ranging from I = 3 to 200 mM (the lowest value corresponding to the left-most points) at pH 8.0: ○ = ovalbumin; △ = calmodulin. Even though the retention of these samples corresponds to large proteins owing to interfacial repulsion, their peak widths are much smaller [*cf.*, condition (upper curve)].

polydispersity obscures the dynamic aspects of peak dispersion. This behaviour of immunoglobulin has been found reproducibly under all conditions studied and immunoglobulin was therefore excluded from further dispersion analysis. A similar observation regarding immunoglobulin heterogeneity was reported previously [73].

In addition, it was observed that aged samples of glycoproteins sometimes gave increased peak widths without notable changes in retention volume. In this event a new sample was employed and the old data were rejected. Any extra pressure drop due to column clogging usually also increased the peak width. Mismatch of the eluent between the column and injected solution also tends to increase the peak width. This may actually be one of the reasons for the poor data quality in Fig. 5, which shows one of the earliest data sets acquired.

Eddy contribution to peak dispersion

Fig. 5 presents data obtained at a single flow-rate with one particular column (TSK6000PW) with different-sized solutes. Peclet numbers can therefore be viewed as a function of diffusional Stokes radius. Regardless of the details of interpretation it is obvious that the presented data below $Pe < 100$ are unaffected by the C-term. On the other hand, data above $Pe > 10$ are unaffected by the B-term of eqn. 4, albeit the B-term couples into eqn. 15. This middle region is thus dominated by the A-term. It is reasonably fitted by the original eqn. 10 with $\varepsilon = 2.2$. However a detailed numerical non-linear least-squares fit reduces it to $\varepsilon = 1.7$. The fitting function actually shown is of course that of eqn. 15 in all instances. As no measurements were conducted at low Peclet numbers, one cannot distinguish between eqns. 15 and 8, nor could the functional form of B (eqn. 16) be tested.

The same analysis was performed with a different column, Superose-12, and is shown in Fig. 6. Again, different-sized solutes at a single flow-rate are plotted. The C-term extends to lower Pe and it is more difficult to view the A-term alone. However, it is clear that eddy dispersion is decisively less than predicted by theory. The *ad hoc* hypothesis of an adjustable ε gives a reasonable fit with $\varepsilon \approx 0.6 \pm 0.2$. The

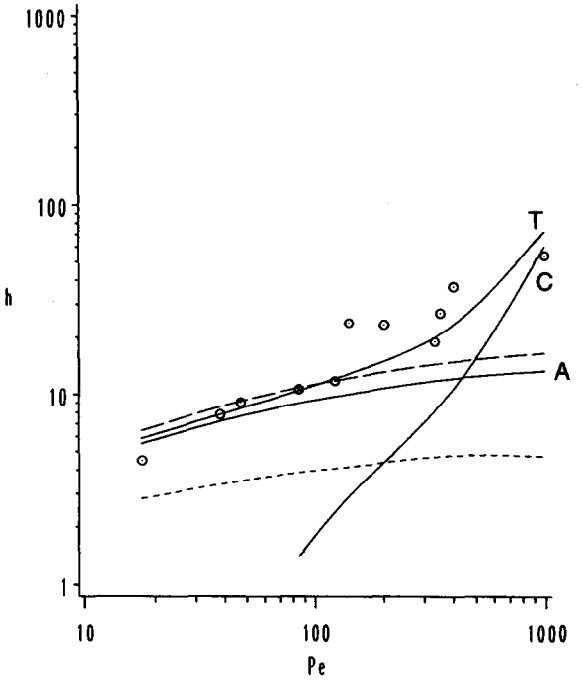

Fig. 5. Van Deemter plot of axial dispersion showing the reduced plate height h as a function of Peclet number Pe. TSK6000PW column 1; eluent, sodium borate (pH 8.25, $I = 4$ mM) in water; flow-rate, 0.2 ml/min; room temperature. Different proteins and viruses (from left to right): vitamin B_{12}, cytochrome c, carbonic anhydrase, bovine serum albumin, catalase, apoferritin, thyroglobulin, phage Qβ, turnip yellow mosaic virus (TYMV), tomato bushy stunt virus (TBSV), tobacco mosaic virus (TMV). Best theoretical representation was obtained from simultaneous fitting of the various theoretical contributions to peak dispersion (for the parameter obtained see Table III). Total dispersion (T) is the sum of an A-term with $\varepsilon = 1.7$ (A) and a C-term (C). For comparison a hypothetical A-term with $\varepsilon = 2.2$ (long dashed line) and $\varepsilon = 0.3$ (short dashed line) are also shown.

compensatory mutual dependence of the three variables is indicated in Table III, which also summarizes the parameters for several other data sets, whose graphical presentation would be repetitious.

Because of the high precision of the data, the parameters for Superose-6 are particularly stable and well determined (Table III). With $\varepsilon \approx 0.5$, the eddy dispersion is similar to, if not even lower than, that for Superose-12. Data for TSK5000PW, on the other hand, are comparable to those for TSK6000PW. It should be noted, however, that a fresh TSK6000PW column yielded a significantly lower ε than the column shown in Fig. 5 (Table III). The deterioration of

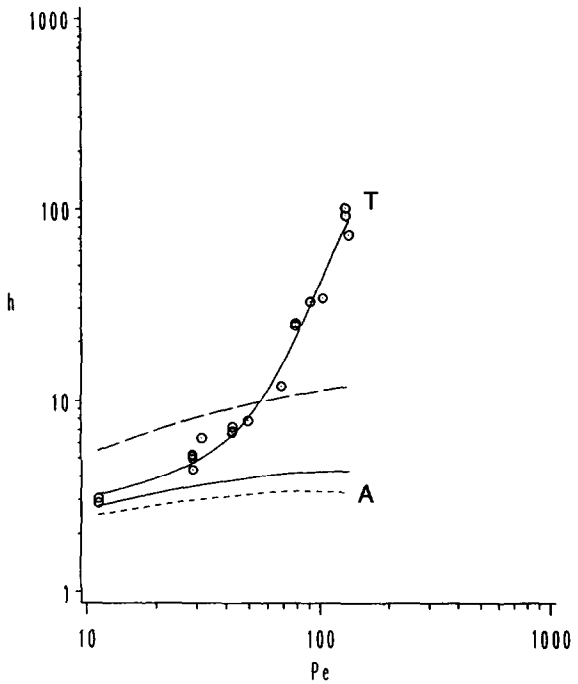

Fig. 6. Van Deemter plot of axial dispersion showing the reduced plate height h as a function of Peclet number Pe. Superose-12; eluent, Tris–HCl–NaCl (pH 8.0, $I = 200$ mM) in water; flow-rate, 0.5 ml/min; room temperature. Same proteins as in Fig. 4 (upper curve) plus a proteolytic fragment of neurofilament protein NF200, which is located near thyroglobulin. Vertically corresponding points are multiple determinations of the same protein. The best theoretical representation was obtained from simultaneous fitting the various theoretical contributions to peak dispersion (for the parameters obtained, see Table III). Total dispersion (T) is the sum of an A-term with $\varepsilon = 0.57$ (flat A) and a C-term (not shown). For comparison, a hypothetical A-term with $\varepsilon = 2.2$ (long dashed line) and $\varepsilon = 0.3$ (short dashed line) are also shown.

columns may therefore be far more limiting for the analysis of dispersion than it is for retention. In any case, eddy dispersion is worse on TSK-PW than Superose. Figs. 5 and 6 include a comparative tracing with $\varepsilon = 0.3$ as the lower limit, corresponding to the data of Basedow *et al.* [35] if the tortuosity difference is neglected. Otherwise Basedow's data actually yield $\varepsilon = 0.5$ and thus match the present Superose data. As the difference between the two series of measurements in Fig. 3 is presumably due to the ε value in eqn. 10, its repeated empirical validation is crucial. Variation of ε does not seem to be related to porosity as a criterion of packing quality as far as eqn. 10 is concerned and a novel parameter of "packing quality" may need to be introduced. Koch and Brady [30] stated that ε depends on the nature of the microstructure. Their value of $\varepsilon = 2.2$ is for ideally smooth spheres. A rougher surface should have a smaller ε. Heterogeneity of the bead sizes, on the other hand, increases A_e [20,34]. Whether this explains the higher values for TSK-PW remains open to speculation.

Hindered transport in the stagnant zone

Once the A-term is known, the experimental values for the C-term may be calculated from the data. However, as they still contain trivial column parameters, it is better to calculate directly the term $\xi_p D_{bulk}/D_{pore}$. This has been done in Fig. 7 for the data for Superose-12. Fig. 7 establishes an exponential size dependence and

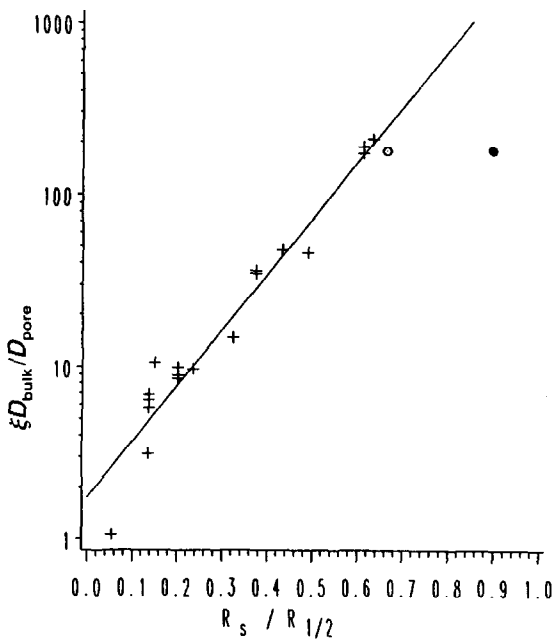

Fig. 7. Obstructed diffusion on Superose-12 in buffered aqueous solution with supporting electrolyte at a flow-rate of 0.5 ml/min at high ionic strength. The various sized proteins are the same as shown in Fig. 6 (+). A 195 bp DNA sample is shown with a diffusional Stokes radius R_s (○) and with a retention radius based on a comparison with proteins, R_{SEC} (●). Data were calculated from experimental values of reduced plate height minus the best-fit A-term, and further divided by the various additional factors of the C-term according to theory. The slope of the semi-logarithmic dependence of obstruction ($\xi D_{bulk}/D_{pore}$) *vs.* aspect ratio ($R/R_{1/2}$) is $\alpha = 7.4$.

TABLE III

PARAMETER FIT OF PEAK DISPERSION

Column	Flow-rate (ml/min)	I (M)	Type of radius in pore	Parameter[a]		
				ε	ξ_p	α
Superose-12	0.500	0.200	Stokes radius R_s	0.57	1.75	7.4
			Stokes radius R_s	0.38	1.90	7.3[b]
			Stokes radius R_s	0.92[b]	1.05	8.3
Superose-12	0.500	0.003–0.2	Calibrated radius R_R	0.92	1.75	7.4
Superose-6	0.250	0.100	Stokes radius R_s	0.52	1.45	5.6
			Stokes radius R_s	0.48	1.55	5.5[b]
Superose-6	0.500	0.214	Stokes radius R_s	0.55	1.50	5.6
TSK5000PW	0.150	0.214	Stokes radius R_s	2.0		
TSK6000PW, column 1	0.200	0.0041	Stokes radius R_s	1.7	1.75[b]	3.5
			Calibrated radius R_R	1.7	1.75[b]	2.0
TSK6000PW, column 2	0.167	0.06 or 0.2	Stokes radius R_s	1.26	1.60	1.0
			Stokes radius R_s	1.26[b]	1.17	2.0[b]

[a] Parameters of eqn. 10 together with eqn. 15, of eqn. 21 and of eqn. 29.
[b] Parameters forced to the specified value whereas the others were optimized.

validates the choice made with eqn. 22. In the case of major convective effects this kind of plot should lead to a plateau value; a minor contribution, however, would simply decrease the slope compared with the universal value proper for obstructed diffusion. Without involving theory, one may simply compare the semi-logarithmic slopes of different columns with varying Cf parameters to survey empirically the occurrence of convection. Exponential relationships were obtained in all instances. Instead of graphical analysis, a simultaneous numerical fit of the raw data was subsequently performed for the various columns and conditions and the resulting α values are given in Table III. The huge differences between the columns studied clearly demonstrates the occurrence of convective but the phenomenological level cannot immediately decide whether the largest observed value, $\alpha = 7.4$, corresponds to pure diffusion or whether ideal obstructed diffusion in the particular geometric network is still larger. Pre-empting the detailed theoretical interpretation of the second part of the discussion section we may record here that Superose-12 at the flow-rate studied safely operates in a purely diffusive regime and $\alpha = 7.4$ is the empirical reference value that is to be compared against theories of obstructed diffusion. Similarly, one may then test the various available theories for the process of convection with the intent of floating all of the apparent α values to a true value of $\alpha = 7.4$.

The observed apparent α values obviously depend crucially on the aspect ratio $R/R_{1/2}$ in eqn. 22. By theory one deals with a diffusion process and R_s would seem to be the obvious choice for the solute radius. This choice is even less critical for the spherical proteins chosen in this investigation as solid spheres ideally have $R_\eta = R_s$. Concerning the pore radius, the choice of average exclusion radius $R_{1/2}$ is certainly a simplification as each solute samples all pore sizes each with different degree of obstruction and larger solutes also preferentially sense larger pores. Alternatively, one could have used individual retention data directly to determine a sliding average cylinder aspect ratio

$$\frac{R_\eta}{R_{1/2}} = 1 - \left(\frac{V - V_{void}}{V_{tot} - V_{void}}\right)^{1/2} \quad (26)$$

If it is correct that retention is defined by a different size criterion, as is implied in eqn. 26 and demonstrated in the next section, this procedure of course fails to provide appropriate aspect ratios $R_s/R_{1/2}$ once $R_\eta \neq R_s$. Reanalysis of the spherical proteins in Fig. 7 in this manner yields $\xi_p = 1.1$ and $\alpha = 7.5$ compared with $\xi_p = 1.7$ and $\alpha = 7.4$ from Table III and ensures the robustness of analysis. The exact match of the Superose-12 data with one of the theories of obstructed diffusion (Famularo) that predicts $\alpha = 7.4$ for ideal monodisperse cylinders should none the less be considered coincidental. In this regard one should note that the pore radii used in analysis had been determined out of context in a publication prior to this investigation and unintentional bias in data handling is hopefully limited by the fact that empirical analysis was completed before the author became aware of the work of Famularo [63] and Rodrigues [141].

Determination of Stokes radii from peak dispersion

Dispersion theory was put forward to argue that retention should be described by diffusional Stokes radii. Peak retention, however, is clearly not determined by R_s but by a term which is R_η or very similar to it most of the time [71,74]. If dispersion is determined by diffusional Stokes radii, as it should be, a difference between retention and dispersion size should be observable with asymmetric molecules and this would establish directly that different kind of processes are involved. At non-vanishing concentrations the situation becomes more complicated as hydrodynamic parameters are concentration dependent. Flexible polymers then diffuse faster inside confinements than solid spheres of equal bulk Stokes radius (see Discussion). The latter was suggested to be true for deformable coiled polymers even at infinite dilute conditions if $R/R_{1/2} > 0.4$. It was then natural to test the SEC dispersion of asymmetric molecules.

Fig. 7 shows that a DNA sample [195 base pairs (bp)] almost matches the protein curve if plotted in terms of its Stokes radius. A more extensive study of DNA restriction fragments, however, indicated a minor tendency towards a smaller peak width w_h than proteins of supposedly same diffusional Stokes radius (unpublished data). While the latter were measured at loads not exceeding 3 μg and in the verified absence of concentration effects on retention volumes, it was not excluded that concentration still had effects on peak width. Overall correlation in terms of Stokes radii is fairly good. The same sample plotted with its chromatographic retention radius R_{SEC} is off the calibration (Fig. 7). In quantitative terms the latter is rejected with a 5σ standard deviation. Hence molecules of different asymmetry but equal retention have different peak widths, as retention is not determined by diffusional Stokes radii. Fig. 7 also contains a coiled protein, a neurofilament fragment designated NF200TP+. It fits well with its Stokes radius determined by quasi-elastic light scattering [74]. In terms of R_{SEC} (not shown), it would be off by a 3σ standard deviation. Both DNA and NF200TP+ are stiff coils and asymmetric. Synthetic chain polymers, however, are usually heterogeneous and thus not well suited for the present analysis. The observations clearly indicate that transport processes do not determine the mechanism of retention.

These examples suggest the means by which R_s may be approximately determined from chromatographic experiments simultaneously with another size measure (the viscosity radius R_η) obtained from retention information. Analysis of both retention and dispersion can be used to decide whether an unknown sample is chain-like with a large ratio of contour length to diameter or has an asymmetric shape. The largest handicap at present is the precision of the data. With the present 1σ variance of 30%, only highly asymmetric samples such as DNA are easily identified.

Ionic strength effects of dispersion

It is well known that the elution of polyelectrolyte samples depends on ionic strength [1,72]. In contrast, only two publications have so far addressed the role of ionic strength on the magnitude of obstructed diffusion [75,76]. The following is the first analysis of the ionic strength dependence of chromatographic peak dispersion. Fig. 4 shows the primary data used for Fig. 6, namely the w_h values as a function of retention

volume for proteins at 200 mM ionic strength on Superose-12 at one given flow rate (0.5 ml/min). If the ionic strength is decreased all of these samples elute earlier. This ionic strength variation is shown in Fig. 4 for two proteins, ovalbumin and calmodulin. Close to the void volume, the peak width drastically decreases but the other peak widths are approximately constant regardless of ionic strength and thus retention volume. Beyond doubt there is some significant difference between a sample at low ionic strength that elutes at this position mainly for reasons of interfacial repulsion, and another one at high ionic strength that elutes at the same volume position mainly because of its large bulk hydrodynamic size.

A w_h plot is somewhat deceiving, however. In contrast to w_h, h does increase with decreasing elution volume since h depends on V^{-2} in eqn. 4. Similarly, C (eqn. 21) depends strongly on retention volume. The A-term, however, almost remains unaffected. It thus becomes straightforward to compute $\xi_p D_{bulk}/D_{pore}$ as a function of ionic strength for a single protein. Surprisingly, this value is not at all a constant, which one might have expected as bulk diffusion coefficients of native proteins hardly change with ionic strength as long as these proteins do not aggregate, dissociate or denature (none of which applies here). Clearly, then, the diffusion rate inside the pores depends on ionic strength. One must therefore somehow define a generalized radius parameter to quantify the data.

At this point recurrence is made to published models of retention [1,72,77]. There are two strategies to use, a reduced pore size or an increased solute size. The truth is, of course, that it is a mutual effect. However, the charge effect on retention depends strongly on solute size, such that the effective reduced pore size would be different for each sample [1]. It therefore makes more sense to tag it to an increased solute term. Quantitatively one then equates the retention volume at low ionic strength to a single effective size R_R that is calibrated via the known sizes at high ionic strength (where R_{IF} is assumed to be negligible). For the sake of terminology it must be added that R_R differs from R_s, R_η and R_{SEC} in principle. Briefly,

$$R_R = R_{SEC} + R_{IF} \quad (27)$$

with $R_{SEC} \geq R_\eta$. For solid rigid objects, R_{SEC} is independent of ionic strength. The dimension of flexible polymers, on the other hand, changes with ionic strength even at infinite dilution under bulk conditions, which causes a variation of R_{SEC} besides the interfacial layer term R_{IF}. R_{IF} encompasses the increase in size due to mutual interfacial repulsion and was discussed in detail previously [1,72,77]. It ideally converges to zero for high ionic strength, even though the influence from hydration forces remains. The R_{IF} term in chromatography is equivalent to the well known concentration effects in bulk solution. Even though solute–solute interactions are eliminated by the experimental conditions of infinite dilution there always remains a finite "concentration" of walls, without which there would not be any SEC effect.

One may therefore presume that a similar effect occurs in transport through confined spaces. In the previous section it was demonstrated that the effective molecular size of retention and dispersion are different except for solid spherical objects. The latter, however, is the case with ovalbumin and calmodulin and for them $R_D = R_R$ since $R_s = R_\eta$. In general terms, the effective size in diffusive dispersion is then

$$R_D = \beta R_s + R_{IF} \quad (28)$$

The complicating introduction of a parameter β is necessary to handle flexible polymer chains. For compact spherical objects, non-deformable rods and stiff coils, $\beta = 1$, as was demonstrated in the preceding section. For flexible polymers such as polystyrene or dextran, $\beta < 1$ at finite concentration and $\beta = 1$ at infinite dilution as long as $R/R_{1/2} < 0.4$ (see Discussion). Note that bulk diffusion coefficients of solid rigid objects, and hence R_s, virtually do not depend on ionic strength once minute amounts of support electrolyte are present [78]. With the parameter R_D at hand to describe the diffusional size inside the pores, where it differs from bulk, one may now quantify the ionic strength variation in a manner similar to regular high ionic strength data. This is done in Fig. 8, which shows $\xi_p D_{bulk}/D_{pore}$ at variable ionic strength as a function of R_R

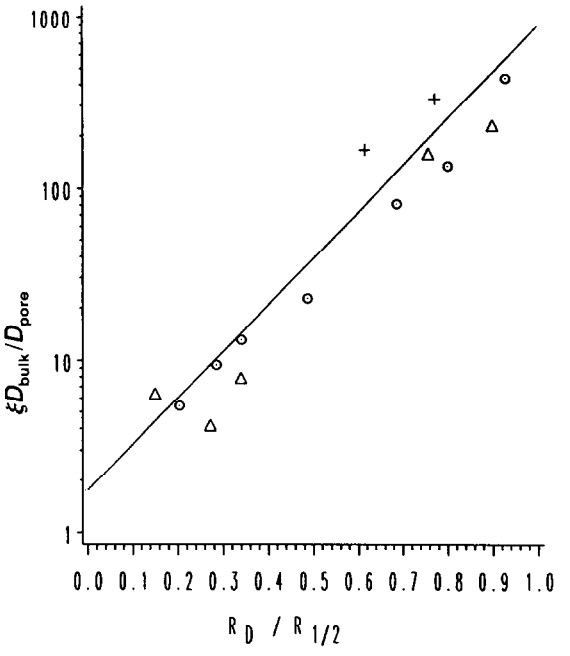

Fig. 8. Obstructed diffusion on Superose-12 at variable low ionic strength. Buffered aqueous solution with supporting electrolyte at a flow-rate of 0.5 ml/min. The aspect ratio is calculated from reference solute sizes matched by their elution volume to include contributions from interfacial repulsion. Lowest ionic strength data are right-most, highest ionic strength data left-most. Data are based on Fig. 4 plus some additional data and were analysed according to theory. ○ = Ovalbumin; △ = calmodulin; + = thyroglobulin.

($= R_D$). The data follow the same type of exponential function according to eqn. 22. Their slope ($\alpha = 6.2$) is, however, lower than that at high ionic strength using the same column ($\alpha = 7.4$). This leads to the following *ad hoc* assumption:

$$D_{pore} = D_{bulk} \cdot \frac{R_D}{R_s} \cdot \exp\left(-\alpha \cdot \frac{R_D}{R_{1/2}}\right) \qquad (29)$$

which is meant to replace eqn. 22. For $R_D = R_s$, eqn. 29 becomes trivially identical with eqn. 22. Note that eqn. 29 may fail if eqn. 25 no longer holds. Via eqn. 29, one obtains for Superose-12 $\alpha = 7.4$ even at low ionic strength. The magnitude of frictional obstruction, expressed in the term α, thus becomes truly independent of the extent of interfacial repulsion (R_{IF} in eqn. 28). The concept of an increased sample size R_{IF}, or of decreased pore size, with decrease in ionic strength, thus shows up both in retention and in dispersion. However, retention and dispersion measure different rotational averages of the solute shape, as demonstrated above, at least as long as convection does not dominate dispersion.

At this point one should reconsider the difference of peak widths for samples of identical retention but different ionic strength (Fig. 4). According to the presented analysis, *C*-terms vary little with ionic strength. The observed large difference in Fig. 4 is therefore due to the Peclet term with which *C* becomes multiplied. This Peclet term refers to mass transport in the interstitial volume and is therefore calculated with bulk diffusion coefficients and R_s. These differ for different-sized samples even though their size R_R inside the pore may be equal.

DISCUSSION

Obstructed diffusion

Obstructed diffusion in SEC is due to four factors: tortuosity, constriction and porosity in the geometry of the porous matrix (collectively just called tortuosity) and frictional drag between a diffusing object and obstructing walls. Flexible polymers are deformed by this frictional drag and their obstructed diffusion becomes an intricate subject of polymer physics. The present data represent the first comprehensive study of obstruction with native globular proteins, ideally applicable to the basic hydrodynamic theories of solid spherical objects.

Tortuosity. Tortuosities of the stagnant zone were calculated from the intercept of plots such as Fig. 7 or obtained directly from global numerical fit of dispersion data (eqn. 4). A value of $\xi_p = 1.5$–1.8 was found for all conditions studied (Table III), but according to Fig. 2c the true tortuosity is 7% larger. Compared with the respective tortuosity factors (Table I), this magnitude implies a significant role of channel constriction (eqn. 19) with a ratio of maximum to minimum radius of *ca.* 2. Tortuosity determined in this manner is, however, extremely sensitive to uncertainties of the aspect ratio $R_s/R_{1/2}$, whereas α values are not, and the accuracy in deriving the pore size variation is therefore limited. Whether Superose-12 exhibits a pore

size variation of at least 1.5 or rather is monodisperse cylindrical must therefore remain undecided. For reticular porous glass of porosity $p_i = 0.48$ a factor of 3 difference was found between microscopic mean radii and mercury porosimetry, which measures minimum radii [79]. A factor of 2 difference was found between mercury porosimetry and radii determined from the volume-to-surface ratio [80]. Others have found smaller ratios for similar glasses [81]. Note that the size dependence of porosity is explicitly treated in the outlined theories for the α term whereas the size dependence of constriction [48,82] is not.

The observed values of tortuosity agree with most of the values reported in the literature (Table IV) and excessive deviations rather indicate systematic experimental difficulties. Particularly values of $\xi_p < 0.93$ are theoretically impossible. Many times problems are obvious, *e.g.*, large values of tortuosity in conjunction with the lack of a dependence on the aspect ratio $R_s/R_{1/2}$, *i.e.*, $\alpha = 0$, amongst the early studies owing to large scatter of data that obscures any size dependence that might have been present. Note that the notion of size-independent D_{pore}/D_{bulk} values [44] persisted in the field of chromatography until about 1983 in spite of theoretical predictions to the contrary and even evidence in related fields (Table IV).

TABLE IV

OBSTRUCTED DIFFUSION

Matrix	Sample[a]	Range of $R_D/R_{1/2}$	Tortuosity, ξ_p	Drag, $\alpha\beta$	Method[b]	Ref.
Frictional drag						
Vycor glass	Linear polystyrene	0.0–1.0	3	0[c]	ND	81
CPG glass	Linear polystyrene	0.0–0.1	1.3	2	QLS	85
CPG glass	Linear polystyrene	0.0–0.2	1.3	2.7	QLS	84
Porous glass	Linear polystyrene	0.0–0.4	1.4	4.1	ND	113
CPG glass	Linear polystyrene	0.1–0.8	1.0	3.4	QLS	67
CPG glass	Star polyisoprene	0.0–0.1	1.3	1.75	QLS	67
CPG glass	Star polyisoprene	0.0–0.1	1.3	3.3	QLS	67
Sephadex	Dextran	0.4–0.7	1.0	2.3	FRAP	110
Sephadex	OM	*ca.* 0.0	1.5	n.a.	ND	100
Porous glass	Water, OM	0.0–0.5	1.7	*ca.* 4	NMR	102
Silica–alumina catalyst	OM	0.1–0.5	2	4.6	ND	50
Vycor glass	OM (dye)	*ca.* 0.5[d]	2.7[c]	*ca.* 6.2	FRS	93
Parallel plates	Latex spheres	0.0–0.1		3.3	QLS	90
Sepharose 4B	Proteins	0.1	1.75 (1.55)	2.1 (3.7[c])	ND	101
Amylose gels	Proteins	0.1–0.4	1.2	1.0	QLS	107
Vycor glass	Proteins	0.0–0.2	2	7.0	ND	81
Frictional drag plus excluded volume						
CPG glass	Linear polystyrene	0.0–0.4	6	0[c]	SEC	48
VITX glass	Linear polystyrene	0.0–0.4	6 (±2)	0[c]	SEC	82
Silica	Linear polystyrene	0.1–0.5	3 (6)	2.3 (1.8)	SEC	95
LiChrospher	Linear polystyrene	0.1–0.8 (0.4)	2 (1)	3 (8)	SEC	19
Hypersil	Linear polystyrene	0.0–0.7 (0.3)[e]	6	1 (3.5)[e]	SEC	18
TSK-G6000H6	Linear polystyrene	0.0–0.6 (0.8)[e]	4	3 (2)[e]	SEC	82
Porasil	Linear polystyrene	0.2–0.9	1.4	2.6[f]	SEC	37
Nuclepore membrane	Linear polystyrene	0.0–0.7	1.0	8.5	SDB	92
Etched mica membrane	Linear polystyrene (high M)	0.0–0.5	1.0	7.6	SD	103
Etched mica membrane	Linear polystyrene (low M)	0.0–0.5	1.0	5.5	SD	105
Etch polycarbonate membrane	Linear polystyrene	0.1–0.6 (0.9)	–	6.3	SD	98,99
Nuclepore membrane	Linear polyisoprene	0.1–0.5	0.7	6.0	SD	87
Nuclepore membrane	Star polyisoprene	0.1–0.5	1.7	6.0	SD	87
Nuclepore membrane	Dextran	0.0–0.1	1.0	0[c]	SD	86
Nuclepore membrane	Dextran	0.1–1.0	0.7	3.6	SD	86
Nuclepore membrane	Dextran	0.3–0.7	0.4	3.4–5.3	SD	94

TABLE IV *(continued)*

Matrix	Sample[a]	Range of $R_D/R_{1/2}$	Tortuosity, ξ_p	Drag, $\alpha\beta$	Method[b]	Ref.
TSK2000/3000SW	Dextran	0.0–0.8	2.9	4.3	SEC	106
Nuclepore membrane	Ficoll	0.0–0.3	1.0	4.4	SD	86
Nuclepore membrane	Ficoll	0.2–0.7	0.6	7.0	SD	86
Nuclepore membrane	Ficoll sulphate	0.0–0.2	0.5 (1.0)	8.4 (4.0)	SD	76
Etched mica membrane	Asphaltenes	0.0–0.8	–	3.9	SD	64
Collodion membrane	OM			>3.3	SD	109
Collodion membrane	OM (sucrose)	0.0–0.2	1	6.2	SD	108
Etched mica membrane	OM (porphyrins)	0.0–0.2	1	5.0	SD	105
Etched mica membrane	OM	0.0–0.2	1	4.6	SD	38
Etched mica membrane	OM	0.2–0.4	1	7.0	SD	38
Etched polycarbonate membrane	OM (inulin)	0.0–0.1	1	8.9	SDB	88
Kidney glomeruli	OM	0.0–0.2 (0.5)	–	4.6	SDB	58
Capillary circulation of perfused hind legs	OM, proteins	0.0–0.6	–	6.7	SDB	111
Cellulose membrane	OM	0.2–0.3	–	4.5	SDB	57
Cellophane membrane	OM	0.1–0.2	–	6.3	SDB	57
Cellophane membrane	OM, proteins, dextran	0.0–1.0	2.0–2.7	–[g]	SD	91
Etched mica membrane	Latex spheres	0.0–0.4	1.0	*ca.* 7.0[h]	SD	75
Nuclepore membrane	Latex spheres	0.1–0.8	1.0	2.5	SDB	89
Millipore membrane	Latex spheres	0.1–0.4	0.08	3.2	SDB	114,128
PSM-800 silica	Silica sol	0.2	*ca.* 2	*ca.* 7	SEC	104
Etched mica membrane	Proteins	0.0–0.4	1	8.2	SD	115,116
Nuclepore membrane	Proteins	0.0 (0.4)–0.8	–	*ca.* 1.0 (2.0)	SDB	96
Agarose gels	Proteins	0.1–0.2	1.0	4.0	SDB	83
Agarose gels	Proteins	0.2–0.5	0.6	*ca.* 7.0	SDB	83
Zorbax-GF250,450	Proteins	0.2–0.5	–	3.1	SEC	97
LiChrosorb diol	Proteins	0.0–0.4	4.2	3.8	SEC	62
LiChrospher silica	Proteins	0.0–1.0	1.9	3.5	SEC	117
TSK-250SW	Proetins	0.1–0.4	1.0	3.5	SEC	73
TSK2000/3000SW	Proteins	0.0–0.8	2.9 (2.0)	4.3 (5.3)	SEC	106
TSK2000SW	Proteins	0.5	*ca.* 2	*ca.* 7	SEC	112
TSK3000SW	Proteins	0.4	*ca.* 1.5	*ca.* 7	SEC	112
TSK-6000PW	Proteins	0.1–0.4 (0.2)[e]	1.6	1.0 (3.0)[e]	SEC	This study
TSK-6000PW	DNA	0.1–0.4 (0.2)[e]	1.5	1.0 (3.0)[e]	SEC	This study
Superose-6	Proteins	0.0–0.6	1.5	5.6 (6.0)[e]	SEC	This study
Superose-12	Proteins	0.0–0.9	1.7	7.4 (7.4)[e]	SEC	This study

[a] OM = Non-polymeric organic molecules.

[b] QLS = quasi-elastic light scattering within the porous material; FRAP = fluorescence recovery after photobleaching within the porous material; NMR = nuclear magnetic resonance; FRS = forced Rayleigh scattering; ND = non-steady state (transient) diffusion with infinite reservoir; SD = steady-state diffusion with finite reservoir, boundary layer effects absent or corrected; SDB = steady-state diffusion with finite reservoir, boundary layer effects non-corrected, which may significantly underestimate α; SEC = dispersion in chromatography (non-steady state diffusion with finite reservoir), α-term may be decreased by convection.

[c] Large scatter in the data prevented detailed assessment. Numerical fit was forced to listed value in order to obtain the complimentary tortuosity (respective drag).

[d] The molecular size given in the original article disagrees with the diffusion coefficients reported in the same article; still, the dye may be adsorbed.

[e] Values in parentheses are for maximum (R_{max}) instead of average pore size ($R_{1/2}$).

[f] Convection explicitly treated in separate term.

[g] Large effect (order of 7 probable) but pore size unknown. Note that exponential relationship is obtained for all data if Stokes radius is used instead of the author's definition of a characteristic radius.

[h] Electrostatic repulsion not corrected with eqn. 29 but by the original authors using certain quantitative energetic assumptions.

Drag and excluded volumes. The present data confirm the applicability of an exponential representation of obstructed diffusion but the observed magnitudes expressed in terms of a coefficient α do not coincide for the different columns studied. These differences are believed to be due to convective transport and the second part of the discussion will elaborate how inclusion of convection theory is able to make all data converge to $\alpha = 7.4$ as the value proper for

obstructed diffusion. This value coincides with the theoretical calculations for cylindrical pores by Bean.

A comparison of this result with the abundant literature on obstructed diffusion [18,19,37,38, 48,50,57,58,62,64,67,73,75,76,81–117] shows that the scatter amongst different studies is almost unacceptable even for methods such as quasi-elastic light scattering or diffusion cell measurements that need not worry about convection (Table IV). Most would probably have opted for the centreline approximation. Interestingly, there is a trend to larger α values in more recent studies. In retrospect, various sources of error must be held responsible for the observed irreproducibility, namely concentration effects, the specific nature of flexible polymers, incorrect or lack of correction for boundary layer resistance, problems of pore size and shape, influence of ionic strength, adsorption and convection. Experiments may have also failed in trivial respects, *e.g.*, proper sampling rate and angle in quasi-elastic light scattering or residual flow (ultrafiltration) in diffusion cell measurements. The remainder of the discussion summarily addresses these problems without possibly passing judgement in all individual cases. Future studies will need to include far more experimental controls to avoid perpetuating this dismal status of affairs.

Preface to Table IV. The earliest experimental study to correlate steady-state diffusion with the aspect ratio of pores in copper hexacyanoferrate(II) precipitation membranes was only qualitative [118]. This is also true of some early chromatographic studies that exemplified the role of diffusion for the mechanism of SEC [119,120]. Many subsequent studies only provided raw data that here are interpreted for the first time. Of those publications that provide theoretical interpretations, only four applied an exponential relationship [50,64,89,91]. For the present comparison, literature data were uniformly reanalysed in terms of eqn. 29 with $R_D = R_s$ except for identified cases of low ionic strength. In some uncertain cases alternative fitting pairs of ξ and α have been included. Since many data are suspected to include concentration effects, Table IV formally lists the product of α times β. Table IV is divided into two sections. First come the methods that are independent of the volume of measurement, such as quasi-elastic light scattering, and therefore measure pure frictional drag, ideally $3.5 \leqslant \alpha \leqslant 4.5$ at least up to $R_s/R_{1/2} \leqslant 0.5$. Current technical limitations prevent measurement by quasi-elastic light scattering at low concentration. Second, there are those methods which for certain boundary conditions [50] also require an excluded volume term; here ideally $5.5 < \alpha \leqslant 7.4$ for solid spheres up to $R_s/R_{1/2} \leqslant 0.6$. Chromatographic dispersion measurements represent a transient diffusion with a finite reservoir and belong to the latter category. Below $R_s/R_{1/2} < 0.1$ the magnitude of obstruction is too small to be reliably measured by SEC and has insignificant weight in wider data sets. All SEC data therefore should yield $\alpha = 7.4$ for diffusion proper. Diffusion cell measurements could in principle provide accurate measurements of the initial slope at low aspect ratios, but none have so far convincingly established the break point which is expected at $R/R_{1/2} = 0.05$ by Famularo and at $R/R_{1/2} = 0.2$ by the centreline approximation (Renkin and others).

Boundary layer resistance. In conventional diffusion measurements across a membrane, a boundary layer of depleted concentration forms whose magnitude depends on the efficiency of stirring and on the pore density. Boundary layer resistance further decreases diffusion rates, more for small than for larger solutes. Hence uncorrected data tend to show decreased values of α and increased tortuosity. While the effect is dramatic for the data of Conlon and Craven [89], it is present also with those of Ackers and Steere [83], which at low aspect ratios superficially fitted to theories with centreline approximation that are now known to underestimate obstruction. Deviations observed in diffusion cell measurements seem to be largely due to insufficient corrections for boundary layers.

For the SEC data in this study, the contribution from boundary layer effects has been explicitly treated with eqn. 12; other studies may, however, have neglected this term and some failed to correct for any of the A-term. Consequently low α-values for SEC in Table IV by themselves do not prove that convective mass transfer did occur.

Flexible polymers. Flexible chain polymers (polystyrene, polyisoprene, dextran) yield lower values of $\beta < 1$ in most studies (Table IV and ref. 121); some, however, find $\beta \approx 1$ at low enough concentrations [87,92,98,99]. Highly branched chain-polymers (Ficoll, star polymers) approach the behaviour for solid spheres (latex, proteins, small molecules), where $\beta = 1$, even at higher concentrations. The present study demonstrates that at least under conditions close to infinite dilution, DNA and asymmetric proteins also approach the behaviour of solid spheres in terms of their equivalent Stokes radii. Values of $\beta < 1$ may be an artifact of sample polydispersity [103]. In addition, values of $\beta < 1$ are expected whenever the polymer is free-draining [94]. Values of $\beta < 1$ have also been rationalized as a truncation of the configurational distribution by sterically excluding the most expanded polymer conformations, which will shift average diffusion coefficients to larger values. Quantitative agreement between theory [62] and experimental polystyrene data [37] was claimed (note that the legend to Fig. 7 in ref. 62 specifies R_G where clearly R_s was used to plot the polystyrene data of ref. 37); in this regard, see also ref. 122. Finally, a complicated theory of flexible chains becoming deformed or even reptating through the pores was advanced [70], but whether they actually reptate is disputed [84,123]. The deformation to a one-dimensional chain is entropically so unfavourable that it requires large driving forces to make the chain enter the pore at all. At infinite dilution such forces may be found in electrophoresis or in ultrafiltration at sufficiently high shear rates (cf., refs. 8 and 124), but not by diffusion. Under infinitely dilute conditions ample evidence is available [1,71] that universal calibration in terms of R_η describes SEC retention with few exceptions that suggest earlier elution as opposed to delayed retention predicted for reptation. However, in semi-dilute solution chain polymers are already deformed and then preferentially enter the pore space where they might reptate [125]. Hence the magnitude of obstruction decreases strongly with increasing concentration of flexible polymers [92,98,99,126]. In fact, a recent theory concluded that $\beta = 1$ for $R/R_{1/2} < 0.4$ as long as flexible polymers are at infinite dilution [69,122]. For higher aspect ratios drag was suspected to deform polymers and enhance transport even at infinite dilution; according to different sets of experiments, however, this ought to happen without increasing retention volumes. One conclusion from this analysis is that concentration effects are significant in the process of kidney glomerular filtration (see ref. 127). Current estimates of the term $\alpha\beta$ for polystyrenes at infinite dilution correspond well with the results of the present study with compact spheres as well as to the theory of Famularo without any need to invoke special partitioning effects (*cf.*, refs. 103 and 122).

Proper choice of pore size. Obstructed diffusion theory depends on pore shape. Even though track-etched mica contains extremely well defined pores, their shape is rhomboidal and obstructed diffusion has not yet been calculated for this case. The observed pattern of α values, which have been defined with equivalent cylindrical pore radii (which different workers have even done in different ways), is not much different from, say, track-etched polycarbonate membranes (Nuclepore), which contain smooth cylindrical pores of fairly monodisperse size.

What values of pore size should be used for polydisperse porous networks? Table IV is based on average values $R_{1/2}$ whenever such data were available, but some workers only reported aspect ratios and may have used other criteria. Further, large solutes probe pores above average size and *vice versa* such that constant mean $R_{1/2}$ may underestimate α. The worst case correction replaces $R_{1/2}$ by R_{max} (Table I). The data from the present study clearly demonstrate that even after such a correction a significant difference remains between the different columns from this study that needs to be explained via convection (Table IV). The uncertainty regarding proper aspect ratios, however, limits quantitative tests of the theory of convection.

Obstructed diffusion of polyelectrolytes at low ionic strength. For the reanalysis of literature data, proper R_D values and eqn. 29 were used at low ionic strength. The only exception is a study of latex as a function of ionic strength [75], which did not provide proper R_{IF} values and consequently could not be analysed in terms of eqn. 29. The non-electrostatic term used by the

workers, which they indirectly based on theoretical assumptions, was included in Table IV. In some instances, effects of ionic strength may have gone unnoticed. In particular, all measurements of latex spheres may have been conducted at insufficient ionic strength and low α values may in part be due to neglect of R_{IF}. Once eqn. 25 no longer holds, ion mobilities further couple in and accelerate diffusion of the macromolecular polyelectrolyte (see also refs. 114 and 128). The present study is the first to relate quantitatively obstructed diffusion that includes a significant contribution from electrostatic interfacial repulsion with independent experimental evidence about their magnitude. The constant α values for Superose-12 at low ionic strength up to $R_D/R_{1/2} < 0.9$ unfortunately cannot be compared with less disputable conditions of high ionic strength which for Superose-12 only reach up to $R_s/R_{1/2} < 0.6$. Most other data on obstructed diffusion do not exceed this margin either.

The demonstration of charge-related effects on size, and thus on aspect ratio, points to a fundamental issue that has already been exemplified for the retention problem at SEC [1]. If hydration forces of significant extent exist, and it is likely that they do, even high ionic strength data will be affected by R_{IF} terms and the concept of size relevant to transport processes in confined spaces may need general revision.

Adsorption. The rate of equilibration in chromatographic beads with solutes was often found to be biphasic, possibly owing to a slower adsorption process [79,120]. Adsorption of molecules delays their migration and thus superficially increases the degree of obstruction. Studied together with non-adsorbing solutes, adsorbing solutes have often been identified and excluded (*e.g.* refs. 50, 102). Other obvious cases were retrogradly excluded (*e.g.*, ref. 129). The questionable data in ref. 94, whatever the reason, seem to have been superseded by ref. 86. Excessively large values of tortuosity may derive from preferential adsorption of the smaller solutes. Small opposite tends that result in superficially increased α values are, however, difficult to identify. While all other sources of error underestimate α, the largest observed values are not automatically the correct ones due to the possibility of adsorption.

One-sided obstruction. The restricted diffusion close to a wall but open to bulk solution on the other side was studied by photon correlation spectroscopy from an evanescent wave [130]. Excess frictional drag is lower than in cavities of parallel plates with same centreline distance, as expected.

Concentrated solutions. It should be mentioned that much earlier an exponential obstruction factor had been derived for the transport of compact objects through concentrated solutions of chain polymers [131,132]. The relationship between polymer concentration and "pore size" unfortunately remains subject to assumptions and it is difficult to arrive at conclusions regarding the magnitude of α. The hydrodynamics of porous matrices undoubtedly provide valuable insight into the properties of concentrated solutions. These, however, are still more complicated [123].

Convective mass transport

As early as 1969 it was reported that axial dispersion is less than predicted by the Van Deemter equation [133], but no reason was given and data were not well analysed. Judged by the results of this study, however, their claim is feasible for their experimental conditions. Later, another study claimed flow through the pores but did not present data [134]. As they were operating at $Cf = 200$ they indeed should have observed convection. Around 1978–82 several studies involved convective mass transport in gas chromatography and SEC, which will now be discussed in more detail with notation adapted to the present style. Intra-pore convection theory seems to have been rederived since [14,135].

First study. Rate-limiting convection may be described by an effective diffusion coefficient according to Taylor–Aries theory. Its convective term $c^2R_{1/2}^2/D$ (c = linear flow-rate, D = three-dimensional diffusion coefficient, $R_{1/2}$ = pore radius) is additive to diffusion proper and leads to the following expression with a numerical factor based on a cylindrical cross-section [136]:

$$C_c = \frac{\xi_p}{69\,500} \cdot \frac{(V - V_{void})}{V^2} \cdot \frac{(V_{column} - V_{void})^2}{V_{void}} \cdot \frac{D_{pore}}{D_{bulk}} \left(\frac{c_{p,eluent}}{c_{p,solute}}\right)^2 \frac{Cf^3}{Pe^2} \quad (30)$$

where c_p is the mean linear velocity of solute or eluent inside the pores and the ratio accounts for effects of hydrodynamic chromatography which include the role of excess drag on convection. Cf is the convective factor defined in eqn. 3. Since diffusion and convection are parallel processes, the final C-term is

$$C^{-1} = C_d^{-1} + C_c^{-1} \quad (31)$$

Equal contributions of convection and diffusion are predicted for

$$Pe = \frac{1}{25} \cdot \frac{D_{pore}}{D_{bulk}} \cdot \frac{c_{p,eluent}}{c_{p,solute}} \cdot Cf^{3/2} \quad (32)$$

where $p_i = 0.34$ was assumed. According to this derivation, convection plays a role at much lower Peclet numbers than initially guessed upon introducing the convective factor term. Owing to the D_{pore}/D_{bulk} term and Pe^{-2} dependence in eqn. 30, convection does not lead to a plateau value but to a pronounced maximum around equality of convection and diffusion followed by a rapid decrease for higher Pe. Such a decrease has been predicted independently for turbulent open capillary flow [137], but the derivation does not apply to low Reynolds numbers. Grüneberg and Klein [138] rejected the Taylor–Aries approach as an artifact of inappropriate assumptions.

Second study. Grüneberg and Klein [138] calculated a term for rate-limiting convection at low Reynolds numbers from random walk theory which is valid as long as the porous zone is still stagnant ($Cf \gg 1$):

$$C_c = l\xi_p \cdot \frac{(V - V_{void})}{V^2} \cdot V_{void} \cdot \frac{c_{p,eluent}}{c_{p,solute}} \frac{Cf}{Pe} \quad (33)$$

where $l = 2$. The same equation but with a numerical factor $l = 3$ was later obtained by Gibbs and Lightfoot [135]. Eqn. 33 replaces eqn. 30 and is used in conjunction with eqn. 31. In their original theory ($l = 2$), equal contributions of convection and diffusion are predicted for

$$Pe = 60 \cdot \frac{D_{pore}}{D_{bulk}} \cdot \frac{c_{p,eluent}}{c_{p,solute}} \cdot Cf \quad (34)$$

where the numerical factor has been modified to account for a tortuosity factor which their original derivation omitted from an equation equivalent to eqn. 21. Accordingly, onset of convection is much later. It eventually leads to a plateau whereas the earlier treatment had predicted a maximum.

However, their own data seem to contradict their theory. On VITX porous glass at $Cf = 5600$ they claimed to observe unusually small C terms compared with VITX glass with smaller pores and thus larger Cf. The reduced plate height h increases linearly with increasing Peclet number and does not (yet) reach a plateau. They claimed to find convection two orders of magnitude larger than predicted by eqn. 33. However, their analysis is flawed and ignores frictional drag which potentially could explain their experimental observations.

Third study. The major novelty of the approach of Rodrigues *et al.* [139] is a complex non-additive coupling between diffusion and convection that replaces eqn. 31 and thus diverges from the additivity theorem of dispersion. Carta *et al.* [140] and Rodrigues *et al.* [141] have adapted this treatment to spherical geometry. Their analysis is equivalent to eqns. 31 and 33 if l is made a variable function of the intra-pore Peclet number λ:

$$\lambda^{-1} = 6 \cdot \frac{D_{pore}}{D_{bulk}} \cdot \frac{c_{p,eluent}}{c_{p,solute}} \cdot \frac{Cf}{Pe} \quad (35)$$

$$\frac{1}{l} = \frac{5}{3}\left(\frac{1}{\tanh \lambda} - \frac{1}{\lambda}\right)^{-1} - \frac{5}{\lambda} \quad (36)$$

According to eqn. 36, one obtains for $\lambda = 1$ $l = 3$, for $\lambda >> 1$ $l = 0.6$ and for $\lambda << 1$ $l = +\infty$; for $\lambda > 10$ the plateau region is reached where $l < 0.7$ and h remains constant with increasing Pe. Rodrigues *et al.*'s equation does not consider the role of inaccessible boundary layers for convection and corresponds in this regard to Van Deemter's original assumption of a constant value for the A-term.

Fourth study. Van Kreveld and Van den Hoed [37] employed an equation similar to eqn. 33 but

based on an effective diffusion whose convective term equals c times a coefficient Cf', which replaces Cf in eqn. 33 and which they adjusted numerically. For Porasil with narrow pores ($R_{1/2} = 13$ nm, $Cf = 5 \times 10^6$, $d = 125$ μm), they observed the onset on convection around $Pe > 10^4$ for polystyrene in the size range $R_s = 3$–12 nm. They reported a plateau in line with eqn. 33 and contradicting eqn. 30. This plateau depends on polystyrene size and their data may be interpreted as

$$Cf' = \frac{240}{l} \cdot \frac{d\ (\mu\text{m})}{R_s\ (\text{nm})} \cdot \frac{c_{p,\text{solute}}}{c_{p,\text{eluent}}} \qquad (37)$$

Hence onset of convection is a factor 500 earlier than predicted by Rodrigues *et al.*, *i.e.*, eqn. 33 with $l = 0.6$ together with eqn. 31, and worse for larger l values. This is in the trend of the claims by Grüneberg and Klein. For the sake of completeness it must be added that the data of Van Kreveld and van den Hoed were obtained at elevated Reynolds numbers, $Re \approx 0.3$–3, *i.e.*, above normal laminar conditions of SEC operation. In fact, one expects $Cf \propto c^{-1}$ in the inertial regime ($Re > 1$) [142]. The numerical factor in eqn. 37 certainly decreases with increasing pore size but no data are available in this regard.

Fifth study. Kirkland [104] claimed intra-pore convection in SEC and refers to Van Kreveld and Van den Hoed but omits quantitative analysis. His data for the PSM-800 silica matrix ($R_{1/2} = 24$ nm, $Cf = 5000$, $d = 6$ μm) exhibit two regimes for the C-term but no plateau. At low flow-rates the C-term crudely corresponds to $\alpha \approx 7$, if the convective term is omitted and falls between the present data for Superose-6 and Superose-12, as would have been expected from the column parameters. At flow-rates above 1 ml/min h continues to increase linearly with increasing Pe but at a decreased rate corresponding to an apparent value of $\alpha \approx 1$, if convective terms are omitted. The same slope is observed for the PSM-500 silica matrix ($R_{1/2} \approx 8$ nm, $Cf = 80\,000$, $d = 7.7$ μm) above 0.2 ml/min. In this instance the initial regime has not been carefully measured but the magnitude of h suggests that it also occurs. Both data sets belong to the low Reynolds number regime ($Re < 0.1$), albeit not as low as in the present study. The slope of $\alpha \approx 1$ implies that the onset of convection is a factor 300 earlier than predicted by Rodrigues *et al.* (eqn. 33) with $l = 0.6$ and corresponds fairly well with eqn. 37. Considering what has been said about eddy dispersion in the mobile zone (A_e-term), these results may not be surprising, except that they are much larger than the Pe variation of A_e. A qualitative picture, however, is emerging: Kirkland's low flow-rate regime corresponds to the conditions and results of the present study; Kirkland's high flow-rate regime corresponds to the initial part of the data of Van Kreveld and Van den Hoed before the onset of their plateau.

Sixth study. Rokushika *et al.* [112] presented dispersion data without interpretation and remarked on their irregularity. For TSK2000SW ($R_{max} \approx 5$ nm, $d = 10$ μm, $Cf \approx 200\,000$) at $Re < 0.03$, their data show a dependency of α on flow-rate, from $\alpha \approx 7$ at 0.1 ml/min to $\alpha \approx 6$ at 3 ml/min. These conditions correspond to $\lambda < 0.01$ and therefore lack convective contributions completely according to Rodrigues *et al.* They are, however, consistent with the second domain of Van Kreveld and Van den Hoed and Kirkland and agree semi-quantitatively with Cf' from eqn. 37. Interestingly, the onset of this effect is later for TSK3000SW.

Seventh study. Afeyan *et al.* [14] recently analysed POROS material ($Cf \approx 90$, $d = 20$ μm) ate $Re < 0.3$ and proposed a theory of convection that is identical with that of Grüneberg and Klein ($l = 2$) without applying it to their data. Judgement is difficult because the paper does not report all the information needed for analysis, but the plateau observed in the range $\lambda = 3$–8 may agree with Rodrigues *et al.* ($l = 0.6$) even though a value as low as $l = 0.2$ cannot be excluded. Lack of a second regime may simply be due to the fact that for such wide-pore material $Cf' > Cf$ rather than the opposite and thus never comes to play.

Shell model. A completely different explanation for a decrease of the C-term with increasing flow rate was put forward by Kubín [143]. He assumed that penetration of the beads is limited to an outer shell of variable thickness because there is insufficient time to establish equilibrium throughout the bead. Others have used Kubín's

model to explain their experimental observation of a decrease of the *C*-term with increasing flow rate [144]. Owing to limitations of space a thorough discussion of this matter is deferred to a forthcoming second part of this series ("The role of transport processes and non-equilibrium in size-exclusion chromatography"). The predictions of Kubín's particular model are, however, briefly compared with the results of this investigation.

This study. Kubín's shell model predicts a maximum around $R/R_{1/2} \approx 0.5$ for the Superose-12 data shown in Fig. 7. In this regard Kubín's model is phenomenologically indistinguishable from the Taylor–Aries theory (first study). At the same time the Kubín model underestimates the effect for TSK6000PW if it alone had to explain the low value of α that is observed in this instance. In order to explain fully the observed dispersion data, convective mass transport must therefore occur.

According to the presented Taylor–Aries theory (see First study) (eqn. 30), Superose-12 data should belong to the diffusive regime. For Superose-6 eqn. 32 predicts a maximum around 100 *Pe*, which is just above the range of measurement. The reported α value should undoubtedly be biased by convection. Finally, TSK6000PW should be entirely in the convective regime. Clearly, no maximum is observed (see Fig. 5) and neither is a plateau. The functional form of eqn. 30 must therefore be doubted.

According to the data of Van Kreveld and Van den Hoed (see Fourth study), the TSK6000PW column would operate in the plateau of convection, which is not borne out by the data. It must be emphasized that according to eqn. 37 even Superose-12, with the same pore size and even smaller beads, should be subject to convective contributions.

The random walk model (see Second study) (eqn. 33 with $l = 2$) predicts that Superose-12 operates in the diffusive regime. Since all data were taken at $\lambda < 0.3$, Rodrigues *et al.*'s analysis (see Third study) claims $l > 10$ and safely excludes convective terms. In analogy with Rokushika *et al.*'s data (see Sixth study), the second convective domain is not yet manifest for Superose-12 at 0.5 ml/min flux. The Superose-12 data consequently represent pure effects of obstructed diffusion. Superose-6 exhibits a slight contribution from convection. The data represent a range $\lambda = 1$–8, which corresponds to $l =$ 0.8–3 according to Rodrigues *et al.* (see Third study) and is difficult to distinguish from the random walk models. The apparent α values for TSK6000PW are significantly decreased but the plateau region lies outside the range of measurement. The available data represent a range of $\lambda = 3$–30 which corresponds to $l = 0.6$–1.2. According to the data of Afeyan *et al.* (see Seventh study) one would not expect much of a second domain for this column. Explicit account of convection increases α to a value around 7 and demonstrates that this magnitude is the true value for diffusive mass transfer of solid spheres in all porous matrices. A value of $l = 2$ is clearly insufficient in this regard and gives preference to Rodrigues *et al.*'s equation (eqns. 33, 35, 36). The large scatter of this particular data set and the wide pore size distribution of TSK6000PW, however, preclude a decisive validation of the details of Rodrigues *et al.*'s equation.

The experimental data in this investigation are based on different solutes run at the same flow-rate. Future study of their flow-rate dependence is expected to resolve the undecided quantitative issue. It is obvious, however, that Rodrigues *et al.*'s analysis does not predict the observation of a second domain of dramatically increased convection. In part this should be related to the neglected Peclet number, Reynolds number and geometric dependence (see A_e-term in Theory section). The observed magnitude and phenomenology (Cf' term), however, is clearly not understood. The cumulative empirical evidence, however, is consistent and leaves no doubt about the crucial influence of convection not only for novel wide pore materials but even for traditional SEC situations.

CONCLUSIONS

Of all theoretical considerations of obstructed diffusion, the numerical results of Famularo come closest to experimental truth and their use is strongly recommended. His calculations are well represented by a logarithmic one-parameter

function for obstructed diffusion in those instances where excluded volume and drag effects occur together, such as in SEC. The parameter then is $\alpha = 7.4$ except for the very initial slope of $\alpha = 5.5$. Drag effects alone are not well represented in this manner. Geometrically simple membrane pores and complex porous networks of variable cross-section behave similarly as far as data quality permits a conclusion. Advanced theoretical efforts in complex geometry are desirable, however, as much as experimental consolidation. The centreline approximation is clearly erroneous and many of its widespread applications, particularly in the field of biological porosimetry, will need to be revised. There is reasonably good evidence that, in the limit of infinite low sample concentration, obstructed diffusion correlates with the diffusional Stokes radius of infinite dilution plus extra interfacial terms due to the finite "concentration" of the pore walls. Deviations to smaller sizes are artifacts of finite sample concentrations, at least for aspect ratios of $R/R_{1/2} < 0.4$. The obstructed diffusion of polyelectrolytes at low ionic strength is fully explained by the role of interfactial effects analogous to their role in SEC retention. As different sizes are derived by retention and dispersion for asymmetric molecular shapes, the mechanism of retention is not determined by transport processes.

Convective mass transport within the stagnant zone occurs in most SEC studies. SEC of large polymers is only feasible because convection substantially improves resolution. Of all theories of convection, the equation of Rodrigues *et al.* comes closest to experimental evidence, but does not explain the occurrence of the manifold increased convection at higher than standard flow-rates that was observed in two other studies and is currently not understood. Consequently, ultra-rapid separations are feasible even with narrow-pore materials without ever exceeding a reduced plate high of $h \approx 100$, which may be sufficient for some process control applications. For those who so far have remained sceptical about the existence of flow-through capillaries in chromatographic matrices, the demonstration of convection also provides evidence for this totally porous nature of the materials. Further, the so-called "stagnant" zone moves slowly through the beads, even though the flow is Cf times less than in the mobile zone.

Analysis of Van Deemter's A-term suggests that the assumption of laminar flow in the mobile zone is invalid. Comparison of different chromatographic columns yields a variation of the A-term by a factor of 3, the origins of which remain to be established. Such variation was formerly attributed to the quality of the column packing and is not explained by the role that theory gives to the porosity parameter. A proper physical description of convection and diffusion in the mobile zone is obviously intimately helpful in formulating the equivalent problem of stagnant zone mass transfer. The theory now seems fit for accurate predictions of reduced plate heights and thus enables *a priori* optimization of resolution and correction of physical dispersion in size distribution analysis. A refined understanding of the mechanism of chromatographic dispersion helps in comprehending the geometric topology of packed beds and porous materials and of its hydrodynamics.

SYMBOLS

a	Mark–Houwink exponent
c	interstitial linear velocity
c_p	intra-pore linear velocity
c^*	overlap concentration
c_{inj}	concentration of the injected sample
d	bead diameter
flux	volumetric flow-rate
h	reduced plate height
k	adjustable parameter in A-term
l	constant or variable factor in C_c
m	exponent that measures fluid conditions
n	net charge of polymer
p	porosity [of the interstitial (p_i) or bead (p_b) zone]
w_h	peak width at half-height
A	Van Deemter term A
A_e	term for eddy dispersion
A_p	term for film resistance of trans-zone transfer
$\langle A \rangle$	average cross-sectional area of a pore

A_{max} maximum cross-sectional area of a pore
A_{min} minimum cross-sectional area of a pore
B Van Deemter term B
C Van Deemter term C
C_c convective contribution to mass transfer term
C_d diffusive contribution to mass transfer term
Cf convective factor
D diffusion coefficient [in bulk solution (D_{bulk}) or in confined pore space (D_{pore})]
I ionic strength
L column length
M generic molecular mass
M_n number-average molecular mass
M_w mass-average molecular mass
N number of plates
P Van Deemter-like term of sample polydispersity
Pe Peclet number (of mobile zone)
R generic radius
R_R effective radius of retention in SEC
R_D effective radius of dispersion in SEC
R_{IF} interfacial contribution to the effective radius
R_{SEC} equivalent shape radius of core body as part of R_R
R_s bulk diffusional Stokes radius at infinite dilution
R_η bulk viscosity radius at infinite dilution
R_{max} maximum pore radius
R_{min} minimum pore radius
$R_{1/2}$ average pore radius
Re Reynolds number
V retention volume
V_{column} total volume of the empty column
V_{tot} total liquid volume of the filled column
V_{void} interstitial volume
Δp back-pressure
Δr film thickness

Greek letters

α key factor in obstructed diffusion
β concentration dependent size compression factor
η solution viscosity
$[\eta]$ intrinsic viscosity
λ Peclet number (of stagnant zone)
ρ density
σ standard deviation
ξ tortuosity [of the interstitial (ξ_i) or pore (ξ_p) zone]
ε adjustable parameter in A_e
$\omega, \omega', \omega_i$ proportionality constants in A-term

REFERENCES

1 M. Potschka, *Macromolecules*, 24 (1991) 5023.
2 R.C. Weast and M.J. Astle (editors), *CRC Handbook of Chemistry and Physics*, CRC Press, West Palm Beach, FL, 59th ed., 1979.
3 M.A. Stadalius, B.F.D. Ghrist and L.R. Snyder, *J. Chromatogr.*, 387 (1987) 21.
4 A.E. Scheidegger, *The Physics of Flow Through Porous Media*, Macmillan, New York, 1957.
5 T.H. Gouw and R.E. Jentoft, in T.H. Gouw (Editor), *Guide to Modern Methods of Instrumental Analysis*, Wiley, New York, 1972, p. 43.
6 R.M. Webber, J.L. Anderson and M.S. Jhon, *Macromolecules*, 23 (1990) 1026.
7 A.A. Zick and G.M. Homsy, *J. Fluid Mech.*, 115 (1982) 13.
8 M. Potschka, *J. Polym. Sci.*, submitted for publication.
9 D.M. Smith and D.G. Huizenga, *J. Phys. Chem.*, 89 (1985) 2394.
10 G. Stegeman, J.C. Kraak and H. Poppe, *J. Chromatogr.*, 550 (1991) 721.
11 D.P. Haughey and G.S.G. Beveridge, *Can J. Chem. Eng.*, 47 (1969) 130.
12 W.J. Moore, *Physical Chemistry*, Prentice-Hall, Englewood Cliffs, NJ, 1972, p. 863.
13 J.H. Aubert and M. Tirrell, *Rheol. Acta*, 19 (1980) 452.
14 N.B. Afeyan, N.F. Gordon, I. Mazsaroff, L. Varady, S.P. Fulton, Y.B. Yang and F.E. Regnier, *J. Chromatogr.*, 519 (1990) 1.
15 N.B. Afeyan, N.F. Gordon, S.P. Fulton and F.E. Regnier, in R.H. Angeletti (Editor), *Techniques in Protein Chemistry*, Vol. 3, Academic Press, San Diego, 1992, p. 135.
16 S.G. Weber and P.W. Carr, in: P.R. Brown and R.A. Hartwick (Editors), *High Performance Liquid Chromatography* (*Chemical Analysis*, Vol. 98), Wiley, New York, 1989, p. 1.
17 B.A. Bidlingmeyer and F.V. Warren, *Anal. Chem.*, 56 (1984) 1583A.
18 J.H. Knox and F. McLennan, *J. Chromatogr.*, 185 (1979) 289.
19 O. Chiantore and M. Guaita, *J. Liq. Chromatogr.*, 5 (1982) 643.
20 J.V. Dawkins and G. Yeadon, *J. Chromatogr.*, 188 (1980) 333.

21 J.C. Giddings, *Dynamics of Chromatography, Part 1*, Wiley, New York, 1965.
22 J.F.K. Huber, *Fresenius' Z. Anal. Chem.*, 277 (1975) 341.
23 C. Horváth and H. Lin, *J. Chromatogr.*, 126 (1976) 401.
24 J.H. Knox, *J. Chromatogr. Sci.*, 17 (1977) 352.
25 P.A. Bristow and J.H. Knox, *Chromatographia*, 10 (1977) 279.
26 G.J. Kennedy and J.H. Knox, *J. Chromatogr. Sci.*, 10 (1972) 549.
27 J.L. Waters, J.N. Little and D.F. Horgan, *J. Chromatogr.*, 7 (1969) 293.
28 J.H. Knox and J.F. Parcher, *Anal. Chem.*, 41 (1969) 1599.
29 J.H. Knox, G.R. Laird and P.A. Raven, *J. Chromatogr.*, 122 (1976) 129.
30 D.L. Koch and J.F. Brady, *J. Fluid Mech.*, 154 (1985) 399.
31 C.L. de Ligny, *J. Chromatogr.*, 49 (1970) 393.
32 G.E. Fleig and F. Rodriguez, *Chem. Eng. Commun.*, 13 (1982) 219.
33 R.N. Kelley and F.W. Billmeyer, Jr., *Anal. Chem.*, 41 (1969) 874.
34 A.J. de Vries, M. LePage, R. Beau and C.L. Guillemin, *Anal. Chem.*, 39 (1967) 935.
35 A.M. Basedow, K.H. Ebert, H.J. Ederer and E. Fosshag, *J. Chromatogr.*, 192 (1980) 259.
36 D.S. Horne, J.H. Knox and L. McLaren, *Sep. Sci.*, 1 (1966) 531.
37 M.E. van Kreveld and N. van den Hoed, *J. Chromatogr.*, 149 (1978) 71.
38 R.E. Beck and J.S. Schultz, *Biochem. Biophys. Acta*, 255 (1972) 273.
39 D.M. Malone and J.L. Anderson, *AIChE J.*, 23 (1977) 177.
40 C.K. Colton and K.A. Smith, *AIChE J.*, 18 (1972) 958.
41 A.A. Kozinski and E.N. Lightfoot, *AIChE J.*, 18 (1972) 1030.
42 M.P. Bohrer, *Ind. Eng. Chem., Fundam.*, 22 (1983) 72.
43 B.D. Mitchell and W.M. Deen, *J. Colloid Interface Sci.*, 113 (1986) 132.
44 J.C. Giddings and K.L. Mallik, *Anal. Chem.*, 38 (1966) 997.
45 W. Heitz and J. Čoupek, *J. Chromatogr.*, 36 (1968) 290.
46 D.M. Andersson and H. Wennerström, *J. Phys. Chem.*, 94 (1990) 8683.
47 L.M. Pismen, *Chem. Eng. Sci.*, 29 (1974) 1227.
48 J.C. Giddings, L.M. Bowman, Jr. and M.N. Myers, *Macromolecules*, 10 (1977) 443.
49 J. van Brakel and P.M. Heertjes, *Int. J. Heat Mass Transfer*, 17 (1974) 1093.
50 C.N. Satterfield, C.K. Colton and W.H. Pitcher, Jr., *AIChE J.*, 19 (1973) 628.
51 E. Glueckauf, *Trans. Faraday Soc.*, 51 (1955) 1540.
52 A.M. Lenhoff, *J. Chromatogr.*, 384 (1987) 285.
53 W.W. Yau, J.J. Kirkland and D.D. Bly, *Modern Size-Exclusion Liquid Chromatography*, Wiley, New York, 1979.
54 H. Faxen, *Anal. Phys.*, 68 (1922) 89.
55 J.D. Ferry, *Chem. Rev.*, 18 (1936) 373.
56 J.D. Ferry, *J. Gen. Physiol.*, 20 (1936) 95.
57 E.M. Renkin, *J. Gen. Physiol.*, 38 (1954) 225.
58 J.R. Pappenheimer, E.M. Renkin and L.M. Borrero, *Am. J. Physiol.*, 167 (1951) 13.
59 A.J. Hurd, R.C. Mocklev and W.J. O'Sullivan, in W.T. Mayo, Jr. and A.E. Smart (Editors), *Proceedings of the 4th International Conference on Photon Correlation Techniques in Fluid Mechanics*, Joint Institute for Aeronautics and Acoustics, Stanford University, Stanford, CT, 1980, pp. 22-1–22-10.
60 J.L. Anderson and J.A. Quinn, *Biophys. J.*, 14 (1974) 130.
61 P.L. Paine and P. Scherr, *Biophys. J.*, 15 (1975) 1087.
62 V.G. Maltsev, B.G. Belen'kii and T.M. Zimina, *J. Chromatogr.*, 292 (1984) 137.
63 C.P. Bean, in G. Eisenman (Editor), *Membranes: a Series of Advances*, Vol. 1, Marcel Dekker, New York, 1972, p. 1.
64 R.E. Baltus and J.L. Anderson, *Chem. Eng. Sci.*, 38 (1983) 1959.
65 H. Brenner and L. Gaydos, *J. Colloid Interface Sci.*, 58 (1977) 312.
66 J. Happel and H. Brenner, *Low Reynolds Number Hydrodynamics*, Prentice-Hall, Englewood Cliffs, NJ, 1965.
67 N. Easwar, K.H. Langley and F.E. Karasz, *Macromolecules*, 23 (1990) 738.
68 R. Tijssen, J. Bos and M.E. van Kreveld, *Anal. Chem.*, 58 (1986) 3036.
69 W.M. Deen, *AIChE J.*, 33 (1987) 1409.
70 P.G. de Gennes, *Scaling Concepts in Polymer Physics*, Cornell University Press, Ithaca, NY, 1979.
71 M. Potschka, *Anal. Biochem.*, 162 (1987) 47.
72 M. Potschka, *J. Chromatogr.*, 441 (1988) 239.
73 Q.C. Meng, Y.-F. Chen, L.J. Delucas and S. Oparil, *J. Chromatogr.*, 445 (1988) 29.
74 M. Potschka, P. Timmins, K. Weber and N. Geisler, in preparation.
75 D.M. Malone and J.L. Anderson, *Chem. Eng. Sci.*, 33 (1978) 1429.
76 W.M. Deen and F.G. Smith, III, *J. Membr. Sci.*, 12 (1982) 217.
77 M. Potschka, *J. Chromatogr.*, 587 (1991) 276.
78 D.L. Edmark, *J. Chem. Phys.*, 62 (1975) 4197.
79 W. Haller, *J. Chromatogr.*, 32 (1968) 676.
80 C.N. Satterfield, C.K. Colton, B. de Turckheim and T.M. Copeland, *AIChE J.*, 24 (1978) 937.
81 C.K. Colton, C.N. Satterfield and C.J. Lai, *AIChE J.*, 21 (1975) 289.
82 J. Klein and M. Grüneberg, *Macromolecules*, 14 (1981) 1411.
83 G.K. Ackers and R.L. Steere, *Biochim. Biophys. Acta*, 59 (1962) 137.
84 M.T. Bishop, K.H. Langley and F.E. Karasz, *Macromolecules*, 22 (1989) 1220.
85 M.T. Bishop, K.H. Langley and F.E. Karasz, *Phys. Rev. Lett.*, 57 (1986) 1741.

86 M.P. Bohrer, G.D. Patterson and P.J. Carroll, *Macromolecules*, 17 (1984) 1170.
87 M.P. Bohrer, L.J. Fetters, N. Grizzuti, D.S. Pearson and M.V. Tirrell, *Macromolecules*, 20 (1987) 1827.
88 J.T. van Bruggen, J.D. Boyett, A.L. Van Bueren and W.R. Galey, *J. Gen. Physiol.*, 63 (1974) 639.
89 T. Conlon and B. Craven, *Aust. J. Chem.*, 25 (1972) 695.
90 P.G. Cummins and E. Staples, *J. Phys. E*, 14 (1981) 1171.
91 C.K. Colton, K.A. Smith, E.W. Merrill and P.C. Farrell, *J. Biomed. Mater. Res.*, 5 (1971) 459.
92 D.S. Cannell and F. Rondelez, *Macromolecules*, 13 (1980) 1599.
93 W.D. Dozier, J.M. Drake and J. Klafter, *Phys. Rev. Lett.*, 56 (1986) 197.
94 W.M. Deen, M.P. Bohrer and N.B. Epstein, *AIChE J.*, 27 (1981) 952.
95 J.V. Dawkins and G. Yeadon, *J. Chromatogr.*, 206 (1981) 215.
96 E. Fuchs and G. Gorin, *Biochem. Biophys. Res. Commun.*, 5 (1961) 196.
97 B.F.D. Ghrist, M.A. Stadalius and L.R. Snyder, *J. Chromatogr.*, 387 (1987) 1.
98 G. Guillot, L. Léger and F. Rondelez, *Macromolecules*, 18 (1985) 2531.
99 G. Guillot, *Macromolecules*, 20 (1987) 2600.
100 S.B. Horowitz and I.R. Fenickel, *J. Phys. Chem.*, 68 (1964) 3378.
101 W. Korthäuer, B. Gelleri and M. Sernetz, *Ann. N.Y. Acad. Sci.*, 501 (1987) 517.
102 J. Kärger, J. Lenzher, H. Pfeifer, H. Schwabe, W. Heyer, F. Janowski, F. Walf, S.P. and Z. Danov, *J. Am. Ceram. Soc.*, 66 (1983) 69.
103 I.A. Kathawalla and J.L. Anderson, *Ind. Eng. Chem. Res.*, 27 (1988) 866.
104 J.J. Kirkland, *J. Chromatogr.*, 185 (1979) 273.
105 I.A. Kathawalla, J.L. Anderson and J.S. Lindsey, *Macromolecules*, 22 (1989) 1215.
106 J.K. Leypoldt, R.P. Frigon and L.W. Henderson, *J. Appl. Polym. Sci.*, 29 (1984) 3533.
107 V.M. Leloup, P. Colonna and S.G. Ring, *Macromolecules*, 23 (1990) 862.
108 E. Manegold, *Kolloid Z.*, 49 (1929) 372.
109 L. Michaelis, *Kolloid Z.*, 62 (1933) 2.
110 E. Poitevin and P. Wahl, *Biophys. Chem.*, 31 (1988) 247.
111 J.R. Pappenheimer, *Physiol. Rev.*, 33 (1953) 387.
112 S. Rokushika, T. Ohkawa and H. Hatano, *J. Chromatogr.*, 176 (1979) 456.
113 M.B. Tennikov, B.G. Belen'ky, V.V. Nesterov and J.D. Ananyeva, *Colloid. J. USSR*, 41 (1979) 526 (Engl.), 603 (Russ.).
114 B.M. Uzelac and E.L. Cussler, *J. Colloid Interface Sci.*, 32 (1970) 487.
115 J.H. Wong, *Ph.D. Thesis*, University of Pennsylvania, 1976.
116 J.H. Wong and J.A. Quinn, in M. Kerker (Editor), *Colloid and Interface Science*, Vol. 5, Academic Press, New York, 1976, p. 169.
117 R.R. Walters, *J. Chromatogr.*, 249 (1982) 19.
118 R. Collander, *Kolloid-Beih.*, 19 (1924) 72.
119 Z. Grubisic-Gallot and H. Benoit, *J. Chromatogr. Sci.*, 9 (1971) 262.
120 P. Fasella, G.G. Hammes and P.R. Schimmel, *Biochim. Biophys. Acta*, 103 (1965) 708.
121 J.S. Schultz, R. Valentine and C.Y. Choi, *J. Gen. Physiol.*, 73 (1979) 49.
122 M.G. Davidson and W.M. Deen, *J. Membr. Sci.*, 35 (1988) 167.
123 G.D.J. Phillies, *Macromolecules*, 19 (1986) 2367.
124 T.D. Long and J.L. Anderson, *J. Polym. Sci., Polym. Phys. Ed.*, 23 (1985) 191.
125 Q.T. Nguyen and J. Néel, *J. Membr. Sci.*, 14 (1983) 111.
126 G. Guillot, *Macromolecules*, 20 (1987) 2606.
127 M.P. Bohrer, W.M. Deen, C.R. Robertson, J.L. Troy and B.M. Bremmer, *J. Gen. Physiol.*, 74 (1979) 583.
128 J.L. Anderson and J.A. Quinn, *J. Colloid Interface Sci.*, 40 (1972) 273.
129 B. Prasher and Y.H. Ma, *AIChE J.*, 23 (1977) 303.
130 K.H. Lan, N. Ostrowsky and D. Sornette, *Phys. Rev. Lett.*, 57 (1986) 17.
131 A.G. Ogston, B.N. Preston, J.D. Wells and J. McK. Snowden, *Proc. R. Soc. London, Ser. A*, 333 (1973) 297.
132 R.I. Cukier, *Macromolecules*, 17 (1984) 252.
133 J.N. Little, J.L. Waters, K.J. Bombaugh and W.J. Pauplis, *J. Polym. Sci., Part A-2*, 7 (1969) 1775.
134 D.J. Nagy, C.A. Silebi and A.J. McHugh, *J. Appl. Polym. Sci.*, 26 (1981) 1567.
135 S.J. Gibbs and E.N. Lightfoot, *Ind. Eng. Chem., Fundam.*, 490 (1986) 25.
136 E.A. Di Marzio and C.M. Guttman, *J. Chromatogr.*, 55 (1971) 83.
137 V. Pretorius and T.W. Smuts, *Anal. Chem.*, 38 (1966) 274.
138 M. Grüneberg and J. Klein, *Macromolecules*, 14 (1981) 1415.
139 A.E. Rodrigues, B.J. Ahn and A. Zoulalian, *AIChE J.*, 28 (1982) 541.
140 G. Carta, M. Gregory, D. Kirwan and H. Massaldi, *Sep. Technol.*, 2 (1992) 62.
141 A.E. Rodrigues, J.C. Lopes, Z.P. Lu, J.M. Loureiro and M.M. Dias, *J. Chromatogr.*, 590 (1992) 93.
142 C.L. Prince, V. Bringi and M.L. Shuler, *Biotechnol. Prog.*, 7 (1991) 195.
143 M. Kubín, *J. Chromatogr.*, 108 (1975) 1.
144 A.E. Hamielec and S. Singh, *J. Liq. Chromatogr.*, 1 (1978) 187.
145 T. Hashimoto, *J. Chromatogr.*, 544 (1991) 249.